geosciences

MDPI

Review

Coupled Zircon-Rutile U-Pb Chronology: LA ICP-MS Dating, Geological Significance and Applications to Sediment Provenance in the Eastern Himalayan-Indo-Burman Region

Laura Bracciali [1,2]

[1] NERC Isotope Geosciences Laboratory, British Geological Survey, Keyworth NG12 5GG, UK; laurabrac74@gmail.com

[2] Department of Earth Sciences, Stellenbosch University, 7600 Stellenbosch, South Africa

Received: 25 August 2019; Accepted: 24 October 2019; Published: 5 November 2019

Abstract: U-Pb dating by LA ICP-MS is one of the most popular and successful isotopic techniques available to the Earth Sciences to constrain timing and rates of geological processes thanks to its high spatial resolution, good precision (absolute U/Pb age resolution of ca. 2%, 2s), rapidity and relative affordability. The significant and continuous improvement of instrumentation and approaches has opened new fields of applications by extending the range of minerals that can be dated by this method. Following the development and distribution to the community of good quality reference materials in the last decade, rutile U-Pb thermochronology (with a precision only slightly worse than zircon) has become a commonly used method to track cooling of deep-seated rocks. Its sensitivity to mid- to low-crustal temperatures (~450 °C to 650 °C) is ideal to constrain exhumation in active and ancient orogens as well as thermal evolution of slow-cooled terranes. Recrystallization and secondary growth during metamorphism and the presence of grain boundary fluids can also affect the U-Pb isotopic system in rutile. A growing body of research focusing on U-Pb dating of rutile by LA ICP-MS is greatly improving our understanding of the behavior of this mineral with regards to retention of radiogenic Pb. This is key to fully exploit its potential as a tracker of geological processes. The latest developments in this field are reviewed in this contribution. The combined application of U-Pb zircon and rutile chronology in provenance studies, particularly when complemented by lower-T thermochronometry data, allows the isotopic characterization of the sources across a wide range of temperatures. The benefits of applying detrital zircon-rutile U-Pb chronology as a coupled provenance proxy are presented here, with a focus on the Eastern Himalayan-Indo-Burman region, where a growing number of successful studies employs such an approach to help constrain river drainage and basin evolution and to infer feedback relationships between erosion, tectonics and climate.

Keywords: rutile; zircon; LA ICP-MS; U-Pb thermochronology; cooling; exhumation; sediment provenance; Eastern Himalaya; Burma; Bengal Fan

1. Introduction

The last couple of decades has witnessed an exponential growth of the number of publications presenting U-(Th)-Pb data [1]. Such a spread has been fueled by continuous improvement of the isotopic dating techniques available to the Earth Sciences, namely: chemical abrasion isotope dilution-thermal ionization mass spectrometry (CA-ID-TIMS [2,3]), secondary ion mass spectrometry (SIMS [4]) and laser ablation inductively coupled plasma mass spectrometry (LA ICP-MS [5]). These employ different analytical set-ups and offer variable degrees of age and spatial resolution (see a detailed review and comparison of these techniques in [6]).

Understanding the advantages as well as the limitations of the available dating techniques (particularly in terms of age and spatial resolution) is key in order to define the best-suited analytical strategy to address specific geological questions. Since all geological samples contain some age variation, the dating method of choice must be appropriate to resolve the temporal and spatial scale of the natural variations. With this in mind, the reader is referred to the detailed assessment of precision and accuracy in geochronology by Schoene and colleagues ([7], in particular their Figures 1 and 2).

In LA ICP-MS analysis, a flat surface of the solid sample is ablated with a pulsed laser in a gas-tight chamber, producing an aerosol that is transported in a carrier gas (usually helium, with addition of argon and nitrogen to enhance signal stability and sensitivity, respectively) to an inductively coupled argon plasma, which vaporizes and converts the particles to ions. The ions are separated in the mass spectrometer based on their mass-to-charge ratio by means of a mass analyzer and quantified by a detector ([5,8] and references therein). A limiting factor of the LA ICP-MS technique is the need for natural matrix-matched, homogeneous in age and well-characterized reference materials. The matrix-dependent U/Pb isotope ratio fractionation occurring during the ablation [9–11] requires compositional and structural homogeneity between sample and reference materials to obtain appropriate calibrations. It follows that LA-ICP-MS dates can only be as good as the homogeneity of the reference materials, the accuracy and precision to which such material is known, as well as the stability of the system during analysis [6].

The advantages of the LA ICP-MS technique are: fast sampling of the target mineral phase, high lateral spatial resolution and precise isotopic ratio measurement. Mineral grains can be separated from the host rock and subsequently mounted in epoxy resin discs and polished to expose their interior (single grain analysis) or ablated in polished petrographic thin sections (in situ analysis sensu stricto, cf. [6]) when it is desirable to preserve the original textural context. Typical laser spot diameters range from 5–10 to 30–50 µm depending on mineral type and initial U concentration. Currently, LA ICP-MS routinely achieves precision of ~2% (2s) for U-Pb [6,12], which is suitable for the large majority of bedrock and detrital studies. CA ID-TIMS is the technique that allows the highest U-Pb age resolution (≤0.1% precision and accuracy at the 2s level of uncertainty). However, the spatial resolution of this method is limited and sample preparation (consisting of acid digestion of the sample and chemical separation of the desired elements) and analysis are time-consuming ([6]). In the case of zoned crystals, micro-sampling (by micro-drilling) has been employed to target intra-crystal age domains. Compared to LA ICP-MS, SIMS offers excellent spatial resolution (sub-µm in depth profiling), absolute U-Pb age precision of 1–2% (2s) and is the least destructive of the three methods thanks to its high sensitivity (useful yield). However, SIMS involves a relatively long analysis duration of at least several minutes versus ~30–40 s of laser ablation analysis. Consequently, SIMS is the optimal technique to use for small volume or valuable samples that cannot be destroyed, whereas LA ICP-MS is much better suited for high throughput detrital samples ([6]).

In light of the features described above and the rapidity and relative affordability of the technique, an impressive amount of U-(Th)-Pb data is currently collected by LA ICP-MS at a very fast pace in many active laboratories worldwide. This has favored and in turn benefited from continuous instrumentation and methodology development [13]. A range of laser systems characterized by different wavelengths and pulse widths can be variably coupled with quadrupole (Q-), single-collector sector-field (SC-SF-) or multi-collector (MC-)ICP-MS instruments. The resulting range of different analytical set-ups, acquisition methodologies and data processing approaches requires a common effort from the LA ICP-MS U-(Th)-Pb scientific community to ensure best practice in handling and interpretation of the data [14].

Historically, the most targeted mineral by LA U-Pb studies is zircon ($ZrSiO_4$), a refractory and widespread accessory mineral in crustal rocks. Zircon contains moderate concentrations of U and Th (typically tens to thousands of ppm) and can accommodate significant amounts of trace elements (e.g., Rare Earth Elements, Y, Ti, Sc, Nb, and Hf), while Pb^{2+} is not incorporated into growing zircon crystals at more than ppb levels under most conditions resulting in negligible initial

(i.e., non-radiogenic, or "common") Pb content ([15,16]). Within a single zircon crystal, different growth zones associated with distinct trace element chemical composition can be preserved. These can be revealed by means of back-scattered electron (BSE) or cathodoluminescence (CL) imaging [17–20] prior to the LA work (Figure 1). Such preliminary microtextural analysis is key to guide the selection of the laser ablation spot locations and to avoid sampling of mixed domains resulting in discordant, geologically meaningless dates.

Since the pioneering studies of Feng et al. [21], Fryer et al. [22] and Hirata and Nesbitt [23], U-Pb geochronology of zircon by LA ICP-MS has paved the way for ground-breaking research applications in the Earth Sciences thanks to the versatility of zircon not only as a time-keeper of multiple geological events but also as a tracer of past geological processes and crustal evolution as recorded in its trace element and isotopic (oxygen, Lu-Hf) composition ([15] and references therein). Petrochronology approaches [24] maximize the recovery and exploitation of such a wealth of compositional (s.l.) information in conjunction with age determination. An effort in this direction has driven the development of laser ablation split-stream ICP-MS (LASS-ICP-MS) analysis, which permits the simultaneous determination of isotopic dates combined with elemental abundances and/or isotopic tracers by splitting the sample aerosol between two different ICP instruments [25].

Along with zircon, a range of other accessory minerals can presently be dated by LA ICP-MS (e.g., monazite, xenotime, baddeleyite, titanite, rutile, apatite, and allanite) as well as rock forming minerals such as calcite and aragonite ([13], and references therein).

Rutile, the most common polymorph of TiO_2, is a widely distributed accessory mineral in medium- to high-grade metamorphic rocks and is particularly widespread in eclogites [26]. The common high concentrations of High Field Strength Elements (particularly, Nb and Ta [27]) in rutile allow insight into rock forming conditions and discrimination between different source lithologies. Rutile can also form at lower metamorphic grade, as a primary accessory mineral of granites and carbonatites, in metallic ore deposits and in quartz veins (see review in [26]). Uranium can be easily accommodated in the crystalline structure of rutile due to the comparable ionic radius and charge to Ti^{4+}, although usually at a lower concentration than in zircon, from as low as ~0.01 ppm to ~100 ppm. As others pointed out previously [28,29], it is a widespread misconception that rutile is generally rich in common Pb. The difficulties in U-Pb dating rutile can rather lie in unfavorably high common to radiogenic Pb ratios in the case of low U content. The concentration of Th in rutile is generally negligible. The Zr content of rutile crystallized in a zircon-saturated environment is dependent on temperature [30–33]. Similarly, the Ti content of zircon is T-dependent [31,34], allowing the application of Zr-in-rutile and Ti-in-zircon geo-thermometers to the study of metamorphic and igneous rocks (e.g., [35–38]).

Both zircon and rutile are resistant to chemical and physical breakdown, hence they tend to be preserved as detrital grains (Figure 1a,b) during the various stages of the sedimentary cycle (including burial diagenesis, see Figure 13 of [39]) which makes them ideal provenance proxies. For their high density (respectively, 4.6–4.7 and 4.23–5.5 g/cm^3 [40]) and diamagnetic nature (although rutile can contain Fe in relatively high proportion) zircon and rutile from the same rock can be recovered together in the "non-magnetic" heavy mineral fraction following the application of standard mineral separation techniques.

This study: (i) reviews progress made in the last decade in the field of rutile U-Pb chronology by LA ICP-MS following the characterization and distribution to the scientific community of natural rutile reference materials; (ii) shows how the U-Pb analysis of zircon and rutile from the same bedrock sample (or cogenetic samples) constrains the thermal and geological evolution in a much more revealing manner than zircon alone; and (iii) emphasizes the benefits of applying detrital zircon-rutile U-Pb chronology as a coupled provenance proxy, with examples from the Eastern Himalayan-Indo-Burman region. The term "coupled" is used in this manuscript to refer to the combined application of the same isotopic technique (U-Pb dating) to zircon and rutile grains from the same sample. It does not imply a co-genetic nature of the two minerals, which may have derived from distinct sources. The different

response of zircon and rutile to thermally-activated Pb volume diffusion and the resulting contrasting geological significance of zircon and rutile U-Pb dates are addressed in Section 3.

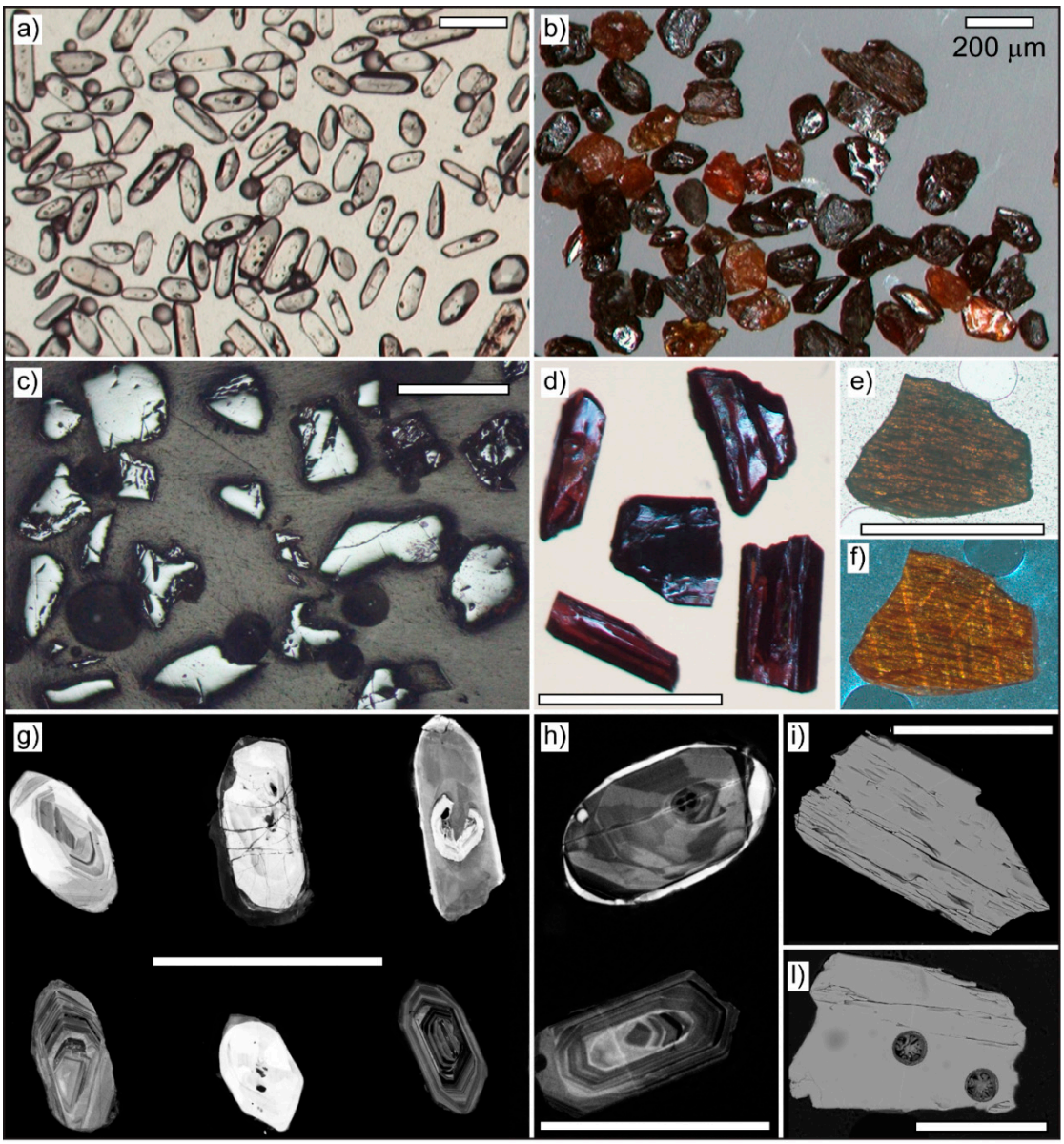

Figure 1. Images of zircon and rutile grains. (**a**) Photomicrograph of polished zircon grains separated from Himalayan-derived modern sand detritus (Mo Chu River, Bhutan). (**b**) Rutile grains separated from sand detritus of the Nanyiqu River, Eastern Himalaya. Note the wide range in color exhibited by the grains, the uneven fracture and the high surface reflectivity (adamantine luster), which is typical of rutile, a consequence of the high refractive index of the mineral. (**c**) Reflected light optical microscopy image of polished R632 [41] rutile grains. (**d**) Rutile grains separated from Sugluk-4 granulite facies quartzite. (**e**,**f**) Optical microphotographs of Sugluk-4 rutile (polarized and crossed polarized light, respectively). (**g**,**h**) SEM-CL images showing an example of the complexity and variety of zircon microtextures observed in individual sandstone samples from the Surma Basin, Bangladesh (respectively, from the Pleistocene Dupi-Tila Formation and the Early Miocene Bhuban Formation [42]). (**i**,**l**) SEM-BSE images showing the lack of zoning in Sugluk-4 and PCA-S207 rutiles, respectively. Note typical laser ablation pits of 50 μm in diameter in (l). White bars are 200 μm in all images.

2. Rutile Reference Materials for LA ICP-MS U-Pb Dating

The first applications of rutile U-Pb chronology by ID-TIMS date back to more than three decades ago [43–47]. These were followed by a large number of studies employing the same technique (e.g., [48–54]). Microbeam dating (by SIMS and LA ICP-MS) lagged behind primarily due to the lack of well-characterized and high-quality natural reference materials necessary for calibration of the analytical method. The first microbeam studies (which employed a SHRIMP, Sensitive High Resolution Ion MicroProbe, a LA multi-collector-ICP-MS or a LA quadrupole-ICP-MS) used an in-house rutile reference material [55], a NIST glass [56] or a zircon reference material [57].

The desired qualities in a primary reference material for U-Pb LA ICP-MS dating are isotopic homogeneity, moderate to high U content (at least tens of ppm to facilitate measurement of the radiogenic Pb isotope signals), negligible initial Pb content (i.e., Pb either introduced during laboratory work or naturally incorporated in the mineral during crystallization [1]) and abundant sample availability for distribution to the scientific community. A thorough chemical and isotopic characterization of each reference material is necessary prior to its distribution and use. The availability of a range of reference materials with variable U content and age facilitates the correction of matrix-dependent isotopic fractionation in unknowns and the validation of the data, particularly for detrital samples in which a wide range of dates can be expected.

Luvizotto et al. [58] and Zack et al. [28] chemically and isotopically characterized two cm-sized monocrystalline natural rutiles: R10 (~1090 Ma) from Gjertsad, South Norway and R19 (~489 Ma) from Blumberg, Adelaide, Australia. The LA U-Pb dating approach of Zack et al. (2011) employed a LA quadrupole-ICP-MS, a laser beam diameter between 50 and 90 µm and pre-selection of rutile grains based on their U-content, discarding grains with <5 ppm U due to the difficulties of measuring low Pb signals. Within-run reproducibility for the Pb/Pb and U/Pb ratios of R10 was reported to be within 3.5% (2RSD). Zack and coauthors applied a ^{208}Pb-based common-Pb correction to samples based on the assumption that radiogenic ^{208}Pb in rutile is negligible due to generally very low Th concentration in rutile. ID-TIMS U-Pb data of R10 uncorrected for common Pb indicate a variable common Pb content in this rutile material [58]; Figure 4e of Bracciali et al. [59]. Chew et al. [60] implemented in the data reduction software package Iolite ([61]) an approach to facilitate the use of primary reference materials with variable, non-negligible common-Pb. This undertakes a common Pb correction using the ^{204}Pb, ^{207}Pb or ^{208}Pb$_{(no\ Th)}$ method for the specified initial Pb isotope composition(s). R10 is unsuitable for laboratories that do not or prefer not to measure ^{204}Pb and/or ^{208}Pb, or that in general prefer not to apply a common Pb correction to the primary reference material. The overall chemical homogeneity and high trace element concentrations of R10 (particularly Zr) favor its use as a reference material for trace element analysis (cf. additional trace element data and discussion in [41]). A second rutile crystal (R10b) was U-Pb dated by a SIMS technique using an O^{2+} primary ion beam coupled with surficial O_2 gas deposition and found to be indistinguishable to R10 within the limits of the microbeam precision [62]. Rutiles R10 and R10b have been distributed to the scientific community and are widely used as primary reference materials for U-Pb dating and trace element analysis.

Bracciali et al. [59] proposed as potential reference materials for U-Pb dating two natural rutiles from granulite facies belts of the Canadian Shield, respectively, from the northern Cape Smith Belt of Quebec and the Snowbird Tectonic Zone, Saskatchewan (Sugluk-4, ~1719 Ma and PCA-S207, ~1865 Ma). ID-TIMS and long-term LA multicollector-ICP-MS U-Pb data of Sugluk-4 show isotopic homogeneity suitable for the two rutiles to be used as reference materials. Conversely, both rutiles show significant intra- and inter-grain trace element chemical variability [41,59], reflecting the detrital origin of their granulite protoliths. The low common Pb content and long-term LA MC ICP-MS reproducibility of (Pb_c-uncorrected) Sugluk-4 ^{206}Pb/^{238}U and ^{207}Pb/^{206}Pb ratios (2–4%, 2RSD, only slightly greater than long-term data for zircon reference materials analyzed within the same timeframe) allow its use as a primary reference material for U-Pb dating without the requirement for correction of common Pb. The approach by Bracciali et.al. [59] permitted dating of ~90% of rutiles in a sediment using a 35–50 µm laser ablation spot-size within samples containing rutile as young as 10–20 Ma, thus obviating

the requirement for U concentration pre-screening and reducing or eliminating rutile selection bias. Unsuccessful analyses were due to poor quality rutiles with predominant common Pb, ^{207}Pb signal below detection, or U content below ~1–2 ppm. Bracciali and co-authors applied the "^{207}Pb-method" using the Tera–Wasserburg diagram to correct for substantial common Pb in individual detrital grains, under the assumption that the only contribution to the offset from concordance was common Pb. Rutiles Sugluk-4 and PCA-S207 have been distributed worldwide to analytical laboratories to be used, respectively, as primary and secondary reference material for U-Pb dating.

A recently developed natural reference material is rutile R632 (~496 Ma [41]) from anorthitic to phlogopitic metasomatites exposed along the Sakena River in southern Madagascar in which rutile occurs as up to 1 mm xenoblasts. In addition to ID-TIMS, Axelsson et al. [41] collected LA single collector-sector field-ICP-MS and LA quadrupole-ICP-MS U-Pb data (using a 90 or 35 μm laser spot-size). Within the level of precision allowed by microbeam methods, rutile R632 proved chemically and isotopically homogeneous, with low common Pb content and high concentrations of Zr (in excess of 4000 μg/g) and U (200–300 μg/g; cf. the U content of R10, ~30–40 μg/g and Sugluk-4, ~30–100 μg/g). For these features, rutile R632 is a suitable reference material for calibration of trace element analysis as well as U-Pb dating.

Importantly, high precision ID-TIMS dating highlighted heterogeneities in the U-Pb systematics of all rutiles currently used as primary reference materials (R10, Sugluk-4, R632). Such variability in Sugluk-4, further confirmed by long-term LA ICP-MS data (~500 analysis over a period of two years), is interpreted to reflect real geological scatter and ascribed to slow cooling and related diffusion, which inevitably induces some intra-grain and inter-grain age variation [59]. Axelsson et al. [41] suggested differences in the closure temperature of the differently sized rutile grains or local alteration for the cause of the scatter observed in rutile R632. The significance of rutile U-Pb dates in relation to volume diffusion of Pb as a function of temperature and crystal size is addressed in detail in Section 3.1.

3. Contrasting Geological Significance of Coexisting Zircon and Rutile U-Pb Dates

3.1. Retentivity of Radiogenic Pb in Zircon and Rutile

In volume diffusion-controlled thermochronology, the concentration of radiogenic Pb within a U- (and Th-)bearing mineral phase reflects the competition between diffusive loss and radiogenic production of Pb isotopes continuously produced by their naturally decaying parents [63,64]. The rate of diffusive loss exceeds the rate of production at high temperatures, and vice versa at low temperatures, i.e., all radio-isotopic systems are subject to resetting at sufficiently high temperatures [65]. The notion of closure temperature (T_c) was introduced to define the boundary of the closed-system vs. open-system behavior, resulting in radiogenic daughter retention (below T_c) or loss (above T_c). Dodson [63] defined T_c as "the T of a system at the time given by its apparent age" and derived an analytical solution to calculate it.

Bulk (or whole grain) thermochronology involves assigning nominal T_c to volume-averaged mineral analyses, hence relating a discrete time-constraint (a date) to a certain temperature (e.g., [66–68]). T_c assumes monotonic cooling and that the effective diffusion radius is the entire grain.

Zircon and rutile generally exhibit remarkably different behavior with regards to retention of radiogenic Pb produced following mineral formation.

Primary zircon can form in high- to low-temperature geological environments and through a variety of processes. In addition to crystallization from igneous melts (typically at temperatures between ~600 and 900 °C [69]), the mineral can form in various metamorphic settings from diagenesis at <100 °C (as tiny and delicate, hardly preserved, overgrowths) to high-grade facies metamorphism. Such growth in the metamorphic realm involves fluid-assisted zircon replacement and modification, crystallization from a Zr-saturated partial melt during anatexis or breakdown of other Zr-bearing mineral phases in response to prograde or—most often—retrograde metamorphic reactions [70,71]. Zircon can also precipitate from hydrothermal fluids at temperatures around 300 °C in ore-forming

systems [72]. Notably, zircon growth generally occurs below the diffusional T_c of Pb in zircon, i.e., at temperatures where Pb diffusion rates are negligibly slow at geological scales. Both experimental studies and empirical studies point to quite high T_c for Pb in zircon (~900 °C), considerably in excess of T_c for other accessory minerals, with the exception of monazite [73,74]. Unless compromised by metamictization or low-temperature dissolution–precipitation (causing Pb loss and discordance), concordant zircon U-Pb dates are thus generally interpreted as formation ages.

In contrast to zircon, volume diffusion of Pb in rutile is effective at temperatures characteristic of the mid- to lower crust. The temperature below which radiogenic Pb is retained in rutile is lower than T_c in zircon by ~300–400 °C [46,75]. A schematic comparison of experimentally determined whole-grain closure temperatures of Pb in zircon, rutile and other accessory minerals [74] is given in Figure 2. As an example, experimental studies on diffusion coefficients in synthetic and natural rutiles predict a whole-grain T_c for Pb diffusion of 620 °C for a spherical rutile of 200 µm and a cooling rate of 1 °C/Myr [75]. Smye et al. [76] reviewed laboratory and field-based estimates of Pb diffusivity through rutile and recalculated diffusivity from previously published empirical data [46,56,77] using a forward modeling procedure (see Figure 3 in Smye et al. [76] and discussion for further details). The resulting estimates of Pb diffusivity from the empirical studies were not only internally consistent but also in excellent agreement with the experimental results of Cherniak [75] between 650 and 750 °C, thus reconciling a seeming disagreement between experimental and empirical estimates for Pb diffusion in rutile.

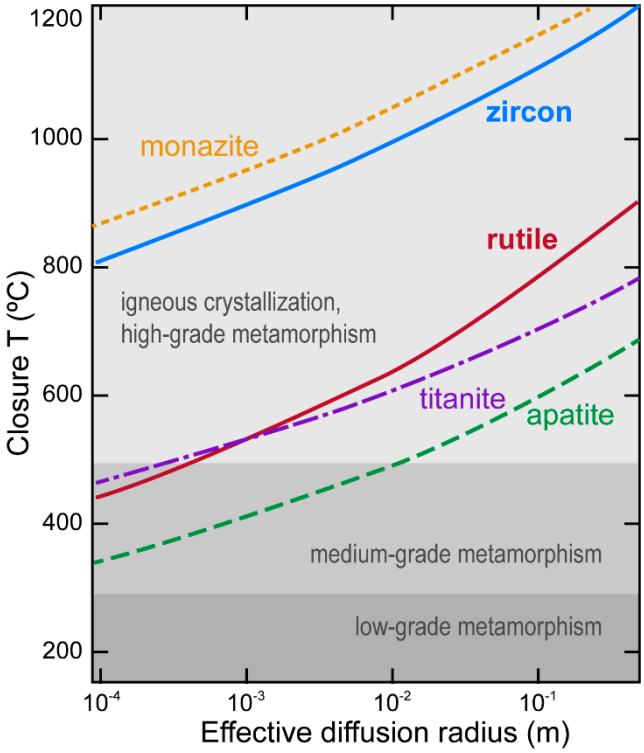

Figure 2. Bulk experimental closure temperatures of Pb in zircon, rutile and other accessory minerals as a function of diffusion ratios for a cooling rate of 10 °C/Myr, calculated by Cherniak and Watson [74] employing Dodson's closure temperature equation [63]. Broad temperature ranges for main igneous and metamorphic events are plotted in the background for comparison. Note the logarithmic scale for the x-axis. Modified after [74], see this reference for data sources. Reproduced with permission from the Mineralogical Society of America. The figure has been slightly modified, but includes all the information and details from the original figure.

For crystals of different size within the same slow-cooled terrane, thermally-activated volume diffusion induces a positive correlation between individual (bulk) U-Pb rutile dates and size of the crystals [46]. This is caused by Pb volume diffusion behavior inducing age gradients within single grains as a result of partial retention of radiogenic Pb and diffusion length's scale dependency (e.g., [56,77]), similar to that observed for other isotopic systems and minerals (e.g., [78]). In other words, T_c varies across the crystal since radiogenic Pb produced within the core of large grains has a physically longer distance to travel than the Pb produced at the rim of the grain (Figure 3b–d).

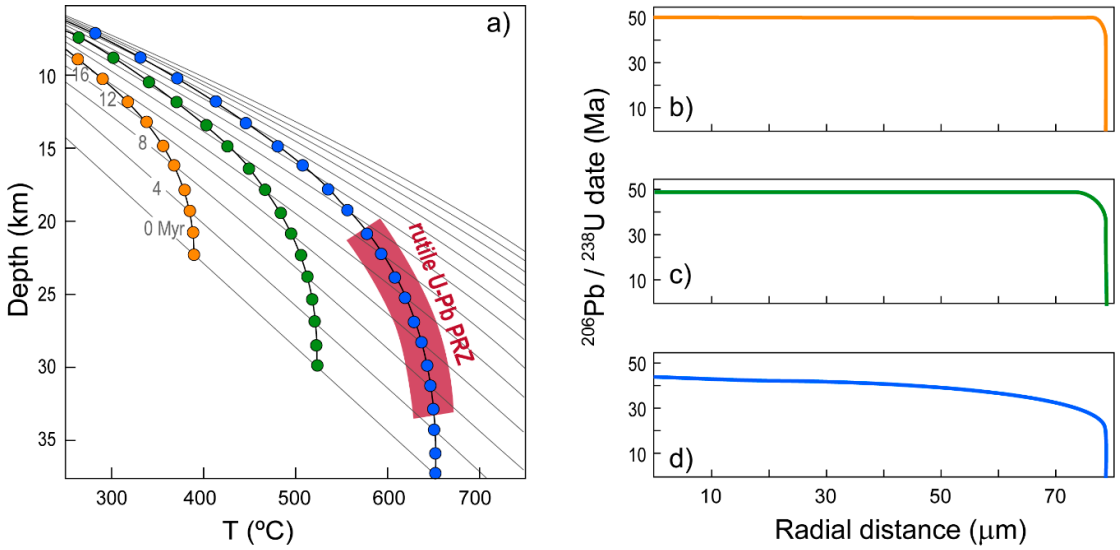

Figure 3. (**a**) Modeled temperature-depth evolution of three rock samples exhuming from different depths (37.5, 30 and 22.5 km). Erosion/exhumation rate: 1 km/Myr; grey lines: geotherms plotted at 4 Myr intervals. Modified after [76], see this paper for further details on thermal model and Pb diffusion parameters used in the calculations. (**b**–**d**) Calculated ^{206}Pb/^{238}U date profiles for single rutile grains in each of the three rocks shown in (a) after 50 Myr of erosion. Note that the whole-grain date for each profile corresponds to an average of the core-to-rim profile. Reproduced with permission from Elsevier. All the information and details are from the original figure.

The notion of "partial retention zone" (PRZ) more comprehensively describes the T-, size- and geometry-dependent open-system versus closed-system behavior of radiogenic daughter isotopes. The PRZ is "the region of T(t) space in which the rate of diffusive loss is comparable to the rate of radiogenic production" (see review in [76]). The extent of the PRZ depends on diffusivity as defined by the Arrhenius law, the cooling rate (hence the crustal setting) and the length scale of Pb diffusive transport through the mineral grain (see Figure 8 of Blackburn et al. [79]). Within the same slow-cooling terrane, the shallowest samples cool quickly through the Pb partial retention zone, yielding old whole-grain dates while the deepest samples reside for a longer time at temperatures that are initially too hot for Pb retention in rutile thus yielding younger dates (Figure 3). Conversely, fast-cooling rates condense the value of diffusivity that may yield partial retention behavior and limit the effects of PRZ residence (with little to no differences between large and small grains).

To resolve potential intra-grain variations as a function of depth into the crystal's interior, age depth-profiling was developed. This approach consists of sampling the mineral at sub-micron intervals by means of SIMS as well as continuously pulsed or single-pulse LA ICP-MS techniques [80]. The numerical inversion of U-Pb rutile date profiles allows the recovery of near-continuous thermal history information from rocks of the middle to lower crust [76].

In addition to thermally-activated volume diffusion, other non-diffusive Pb intragrain transport mechanisms such as recrystallization and secondary growth during metamorphism and the presence of grain boundary fluids of variable chemical composition can affect the U-Pb isotopic system in

rutile and other accessory phases including zircon and monazite (e.g., [77,81]). As re-crystallization involves re-ordering of disordered portions of the crystal lattice, it can promote loss of incompatible elements including radiogenic Pb. Disturbance to the U-Pb isotopic composition of rutile associated with diagenetic processes has also been suggested to occur in rutile (e.g., [82]). Additionally, even in the case of pure Pb diffusive behavior, a mineral enclosed within another phase of limited diffusivity (e.g., garnet) can be subjected to armoring effects limiting or preventing the diffusion of the radiogenic isotopes in response to a thermal event ([67] and references therein).

When applying depth-profiling, caution must be exercised to ensure that measured core-rim radiogenic Pb concentration profiles are diffusive in nature and not influenced by other processes such as recrystallization, secondary growth, occurrence of inclusions or exsolution lamellae of other mineral phases such as Fe-oxides and zircon. In this regard, microtextural observations and trace element analysis can help to discriminate between diffusive and non-diffusive Pb transport mechanisms in accessory phases ([76,83]).

Whole-grain and depth profiling volume-diffusion controlled U-Pb thermochronology of rutile are powerful isotopic tools to constrain cooling following medium-high temperature thermal events related to a wide range of processes such as burial, thrusting, rifting or magmatism. Thus rutile, similar to other minerals whose isotopic systems are sensitive to mid- to low-crustal temperatures (~450 ° to 650 °C, i.e., corresponding to crustal depths in cratonic regions of ~20 to 50 km), can serve as a U-Pb thermo-chronometer and is therefore widely used to estimate duration or rates of crust exhumation (e.g., [84–87]). On the other hand, zircon (similar to other minerals generally forming at temperatures lower than the closure temperature of the isotopic system of interest) is dated by the U-Pb method to obtain absolute time constraints on geological events associated with its formation and is generally referred to as a geo-chronometer. It should be noted however that rutile formation ages, although rare, can be preserved in the cores of large grains [29] and zircon can behave as a thermo-chronometer in regions of the lithosphere cooling from ultra-high temperature conditions [73]. Of particular interest to the Earth Sciences are studies aimed at estimating exhumation rates of deep-seated metamorphic and plutonic rocks in active and ancient orogenic belts as well as long-duration cooling of cratonic lower crust (e.g., [49,52–54,76,79,80,84–90]).

An increasing body of scientific evidence shows that, particularly under conditions of slow cooling, rutile in bedrock samples typically records younger U-Pb dates than coexisting zircon (Section 3.2). In light of the different significance of U-Pb dates in zircon and rutile, the conjunct application of the two chronometers hence provides much more robust temporal and thermal constraints on geological events and processes than when each chronometer is used alone, as further discussed in Sections 3.2 and 4.

3.2. Coupled Zircon–Rutile U-Pb Chronology Applied to Bedrock Studies

This section presents published U-Pb data of coexisting rutile and zircon from geological settings variably characterized by very slow to very rapid cooling rates (summarized in Figure 4). The results of these studies show the versatility and complementarity of coupled zircon-rutile U-Pb chronology in helping to constrain lithospheric evolution.

Mezger et al. [46] determined by ID-TIMS concordant U-Pb dates in rutile from upper amphibolite to granulite facies metapelites of the Archean Pikwitonei domain (Manitoba) and the Proterozoic Adirondack terrane (New York). Within the same domain, U-Pb dates were significantly younger than coexisting U-Pb dates of zircon, i.e., 2330–2430 (rutile) vs. 2598–2695 Ma (zircon) in the Pikwitonei domain and 1005 (rutile) vs. 1155–1420 (zircon) and 1161 Ma (monazite) in the Adirondack domain (Figure 4). Rutile dates were also younger than U-Pb dates for monazite and sphene as well as Ar-Ar dates for hornblende, but older than Ar-Ar dates for biotite. The authors used the known nominal T_c for these isotopic systems to estimate a time-integrated cooling rate for the Adirondack Highlands of 1.5 °C/Myr between 1030 and 800 Ma and assigned values of T_c of 380 and 420 °C, respectively, for rutile with diameters of 140–180 and 180–420 μm. These estimates were later upwards revised to 500 and 540 °C by Vry and Baker [56] who also collected Pb-Pb ages (by LA MC-ICP-MS, using a

spotsize of 300 µm) in rutile from granulite facies rocks of the Reynolds Range, Australia. These were ~1544 Ma, i.e., 30–50 Myr younger than coexisting monazite (1579–1601 Ma) and zircon overgrowths (1596–1571 Ma). The cooling rate established for the Reynolds Range was ~3 °C/Myr.

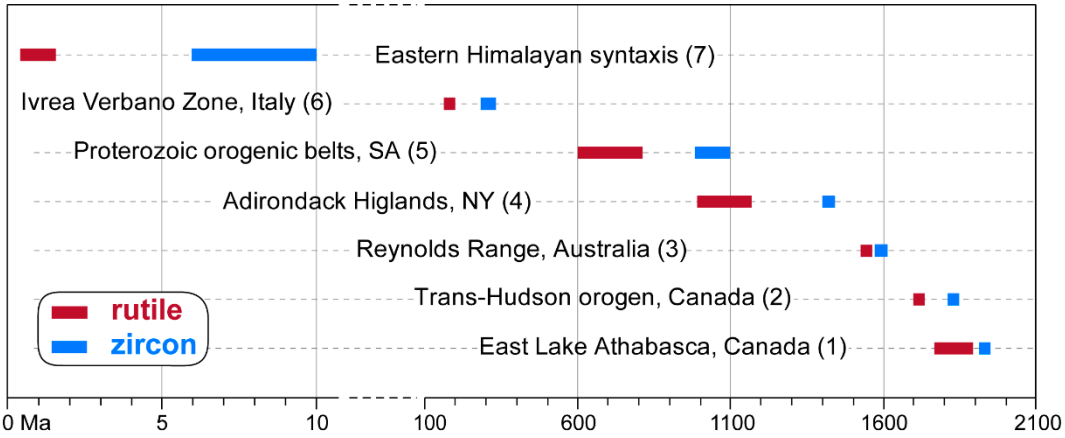

Figure 4. Schematic summary of U-Pb zircon and rutile data from a range of geological settings of different age. See text for details. Rutile data from: (1) [85]; (2) [59]; (3) [56]; (4) [46]; (5) [49]; (6) [89]; and (7) [91]. Zircon data: Same reference as for rutile or references therein.

Schmitz and Bowring [49] observed discordant Proterozoic rutile (with upper intercepts of 1.8 to 1.0 Ga, ID-TIMS data) in kimberlite-borne Archean lower crustal granulite xenoliths from within the cratonic continental lithosphere beneath southern Africa. Zircon discordia arrays in the same samples had 2.9 to 2.7 Ga upper intercepts. Conversely, in Proterozoic (1.1 to 1.0 Ga as determined by zircon and monazite ages) granulite xenoliths from the craton-bounding orogenic belts, rutile defined discordia arrays with Neoproterozoic (0.8 to 0.6 Ga) upper intercepts and Mesozoic lower intercepts (Figure 4). In combination with coexisting titanite and apatite dates, Schmitz and Bowring interpreted the results as a record of post-orogenic cooling at an integrated rate of approximately 1 °C/Myr, and subsequent variable Pb loss in the apatite and rutile systems during a Mesozoic thermal perturbation. Modeling of the diffusive Pb loss from lower crustal rutile constrained the temperature and duration of such perturbation to be <550 °C for ca 50 kyr, thus indicating a protracted manifestation of lithospheric heating likely related to mantle upwelling and rifting of Gondwana during the Late Jurassic to Cretaceous rather than simply a kimberlite-related magmatic phenomenon.

Similar to the previous study, rutiles from minette-borne xenoliths (sampling the Archean lower crust of the Medicine Hat Block in Montana) were used by Blackburn et al. [79,88] to constrain the time-temperature evolution of a sector of the North American lithosphere. In gneissic xenoliths, rutile was recognized to be part of the peak metamorphic assemblage corresponding to 0.8–1.3 GPa and 900 °C, hence grown at temperatures well above those of Pb retention in rutile. Zircon yielded dates between 2.7 Ga and ~1.8 Ga (the latter being the timing of the main thermo-tectonic event in the region) in agreement with previously published data. Single grain rutile analyses from three xenoliths sampled at different lithospheric depths defined discordant curvilinear arrays compatible with a slow-cooling model. The upper intercepts (at ~1.8, 1.5 and 1.0 Ga, respectively, for the shallowest to deepest sample) were interpreted to mark the timing each sample first entered the PRZ. Forward modeling of U-Pb data showed that for cooling rates slower than 10 °C/Myr the effect of grain size causes a dispersion of data along Concordia, with smaller grains yielding younger dates, while for rates of ~ 10 °C/Myr or faster such differences do not occur. For cooling rates slower than ~0.25 °C/Myr (implying a long time spent within the PRZ, as in the case study from Montana) U-Pb data not only are dispersed according to grain sizes but yield extended discordant arrays highly asymptotic to Concordia. In the case of such slow-cooling rates, this also results in a large apparent offset between the $^{206}Pb/^{238}U$ and $^{207}Pb/^{235}U$ systems due to the higher production rate of ^{207}Pb manifested in a relative excess in retained ^{207}Pb.

The U-Pb data presented by Blackburn et al. show that cooling of the Archean continental lithosphere in the Montana study area occurred at rates <0.25 °C/Myr over ca. 1 Gyr.

Many studies have focused on the East Lake Athabasca region (Saskatchewan, Canada) spanning the central segment of the Snowbird Tectonic Zone (a high amplitude gravity anomaly in the Canadian Shield) and exposing a broad area of high P granulites. Work in the area documented the importance of 1.9 Ga metamorphism and subsequent exhumation of deep-crustal rocks [92–94]. Zircon U-Pb ID-TIMS data from East Lake Athabasca mafic and felsic granulites testify to a ~2.55 Ga high-pressure granulite facies event (1.3 GPa, 850 °C) recorded by the dominant mineral assemblage, followed by subsequent zircon recrystallization and minor secondary zircon growth during a second high-pressure granulite facies event (1.0 GPa, 800 °C) at ~1.90 Ga [52,95]. Rutile from various domains of the East Lake Athabasca region [52,85] yielded ID-TIMS U-Pb dates in the range 1.78–1.88 Ga (Figure 4). These data were used along with titanite and apatite U-Pb data and Ar-Ar hornblende, biotite and muscovite data to reconstruct a multi-stage exhumation of the lower continental crust in this sector of the western Canadian Shield. The rutile reference material PCA-S207 (~1865 Ma [59]) was separated from a granulite facies paragneiss from the Southern Domain of the East Lake Athabasca region.

Sugluk-4 rutile [59] was separated from a granulite facies quartzite from the Ungava segment of the Trans-Hudson orogen of Canada, a Paleoproterozoic collisional belt formed between 2.0 and 1.8 Ga following the closure of the Manikewan Ocean [96,97]. The Ungava segment is a ~ 400 km long belt which preserves metaplutonic and metasedimentary thrust sheets (the Narsajuaq arc and Cape Smith belt). The metasedimentary rocks of the Sugluk Group reached peak granulite facies conditions of ~7–8 kbar and >800 °C [98]. Turbiditic sedimentary rocks and the Sugluk-4 quartzite from this location yielded an assemblage of detrital zircons ranging in age from 1832–1840 Ma (interpreted as derived from the 1.82–1.84 Ga plutonic rocks of the Narsajuaq arc) as well as Archean zircons (ID-TIMS U-Pb data [2,99]. Metamorphic overgrowths at 1825–1829 Ma on zircon cores older than 2230 Ma in a garnet-bearing orthogneiss recorded granulite facies metamorphism. A garnet-bearing orthogneiss gave 1815–1820 Ma monazite and 1792 Ma xenotime suggesting a protracted period of slow-cooling from high metamorphic grade to at least 1758 Ma, the age of igneous zircons from a granitic dyke cross-cutting all the elements of the orogen. Within this context, the best estimate for the age of Sugluk-4, 1719 ± 14 Ma (weighted average of ID-TIMS data [59]), testifies to the slow cooling of the Ungava terrane (Figure 4). The intra- and inter-grain age variation of Sugluk-4, with a long-term reproducibility only modestly worse than long-term data for zircon reference materials, reflect real geological scatter caused by slow cooling-related diffusion.

In contrast to the cases of slow-cooled terranes presented so far, the easternmost syntaxial termination of the Himalayan orogen provides a striking example of extremely rapid cooling and exhumation within the India-Asia collision geodynamic framework (Figure 5a).

The eastern Himalayan syntaxis is characterized by exceptionally young (from 10 to <1 Ma) mineral growth and cooling ages of different isotopic systems (e.g., [100–107]). These document Late Miocene to Pleistocene structural, metamorphic, igneous and exhumation events related to the development of the Namche Barwa syntaxial antiform and its rapid exhumation and erosion, which have generated wide interest and debate amongst the Earth Science community with a large number of published studies (see [84,106] for a review). Within the Indian plate of the syntaxis are high-grade metamorphic rocks, locally at granulite facies. A volumetrically-limited melt production in response to partial melting during decompression is recorded by <10 Ma zircon U–Pb dates of granitic dykes and leucosomes occurring in the Namche Barwa–Gyala Peri massif. The timing of emplacement of these granitic melts overlaps the ~5–8 Ma U–Th–Pb dates of monazites separated from the matrix of metapelitic rocks. U–Pb titanite dates from the core of the syntaxis are 4.9 ± 3.9 and 2.8 ± 1.4 Ma, Ar-Ar biotite dates are as young as ~1 Ma, fission track zircon and apatite dates and (U-Th)/He zircon dates are as young as <1 Ma. U-Pb rutile data from granulite facies metapelites in the Namche Barwa massif and detrital rutile in the modern detritus eroded from the syntaxis were respectively 1.4 Ma and ~0.5 Ma, indicating that rocks within the core of the syntaxis were at ~600 °C only 1–2 Myr ago [84].

In the latter sample, detrital Ar-Ar white mica peaked at ~0.4 Ma. The thermochronology data were used by Bracciali et al. [84] in a numerical model of heat flow and erosion to model the path of rocks from peak metamorphic conditions of ~800 °C to <250 °C. The results supported the interpretation that exhumation of the north-easternmost part of the syntaxis occurred in the Pleistocene at rates of at least 4 km/Myr, with bedrock erosion of 12–21 km during the last 3 Ma [84].

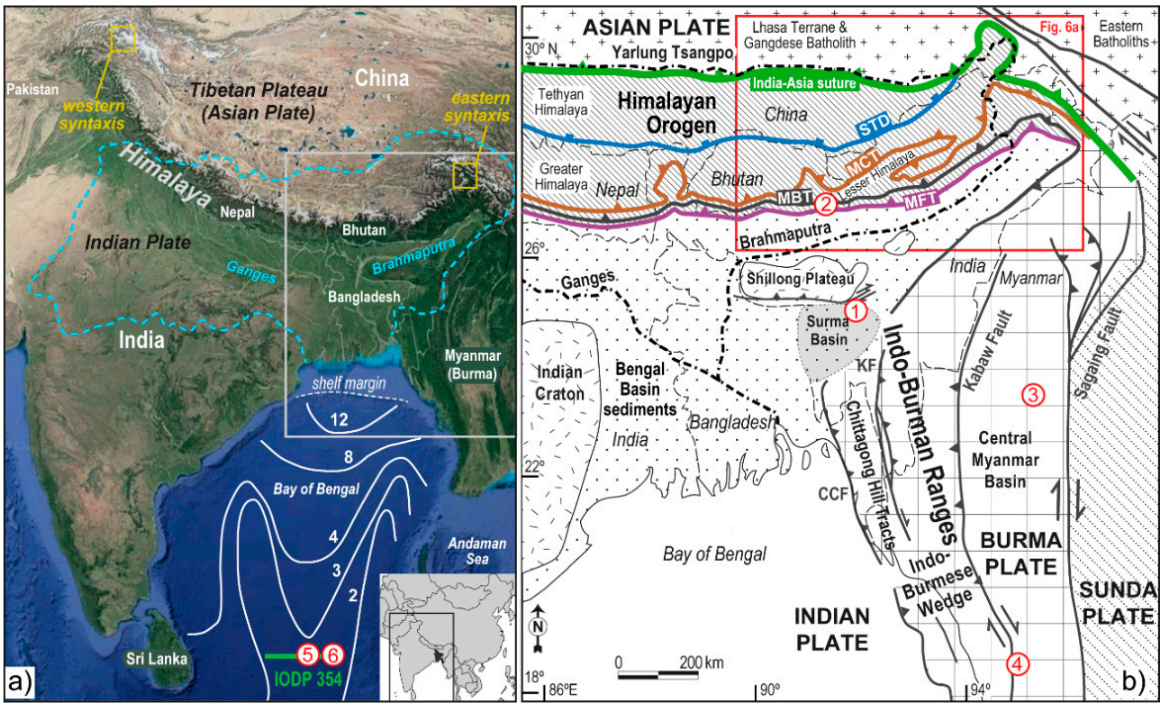

Figure 5. (**a**) Main geographic elements of the Himalayan-Tibet region superimposed on a Google Earth image. Inset shows the location of the region in Eastern Asia. The boxed area corresponds to (**b**). The dashed turquoise curve outlines the combined Ganges-Brahmaputra drainage basin contributing to the Bengal fan sediments. Solid white lines are post-Paleocene Bengal Fan thickness contours in km from [108]. (**b**) Schematic geological map of the Eastern Himalayan-Indo-Burman region showing the Asian, Indian, Burma and Sunda Plates and their main tectonic boundaries. The India–Asia suture separates the Lhasa Terrane from the Indian Plate to the south. This includes the Himalayan Orogen, the Indian Craton and the Bengal Basin sediments. The Indo-Burman Ranges marks the boundary between the Indian and Burma plates. The red box corresponds to map of Figure 6a. Numbered circles indicate location of (surface outcrop or sub-surface) stratigraphic sections from: (1) Surma Basin [42,84]; (2) Himalayan foreland (Siwalik Group, Dungsam Chu section [109]); (3, 4) Central Myanmar Basin [110]; and (5, 6) Bengal Fan (IODP Expedition 354 [108,111]. U-Pb zircon and rutile data from these studies are presented in Figures 8–11.

Detrital data indicate that rutile U-Pb dates near the western side of the southern syntaxis are ≥9 Ma [84] as further detailed in Section 4. Accordingly, U–Pb analyses of rutile which grew at or close to peak temperature conditions in granulites and amphibolites from juxtaposed litho-tectonostratigraphic units within the Greater Himalayan Sequence (GHS) of NW Bhutan yielded LA MC-ICP-MS U–Pb lower intercept cooling ages of ~10–11 Ma [112]. The numerical diffusion modeling of these data suggests rapid cooling from peak temperature conditions of ~800 °C at 14 Ma (constrained by U-Pb monazite data) in the granulite-bearing unit and ~650 °C at 12 Ma in the amphibolite-bearing unit.

Zack et al. [28], Smye and Stockli [80], Ewing et al. [83] and Smye et al. [89] U-Pb dated rutile from the Ivrea–Verbano Zone (IVZ), northern Italy ([29], and references therein). The IVZ exposes an attenuated section through the Permian lower crust that records high-temperature Cambrian metamorphism under lower crustal conditions, Permian magmatism (Mafic Complex, ca. 288 Ma),

Jurassic opening of the Alpine Tethys ocean (starting at ~182 Ma) and subsequent mantle exhumation and eventually exhumation during the Alpine orogeny [113]. Regional granulite facies metamorphism is constrained by U–Pb zircon geochronology to between 295 Ma and 319 Ma [114,115] and peak metamorphic conditions for the granulite facies metasediments to 770–940 °C and 6–10 kbar. Rutile formation is attributed to the break-down of biotite in granulite-facies paragneisses. Zr-in-rutile temperatures of 750–800 °C, with a thermal maximum of >900 °C, demonstrate that rutile formed during Variscan granulite facies conditions [115].

LA ICP-MS depth profiling analysis of unpolished rutile grains (up to 0.5 mm wide) from granulite facies metapelites from Val d'Ossola revealed monotonically increasing $^{206}Pb/^{238}U$ dates from 140 Ma to 180–190 Ma over the outer ~15 µm after which no further age increase was observed [80]. Single spot ages measured between 20 µm and 100 µm from the visible edges of polished grains yield a weighted average of 184 ± 4 Ma, within uncertainty of both the plateau age of the depth profile and the (LA quadrupole-ICP-MS) pooled age of 181 ± 4 Ma obtained for large rutiles from the Val d'Ossola [28]. Smye et al. argued that the preservation of ~180–190 Ma plateau ages within 15 µm of rutile grain edges and the results of a numerical model inverting the $^{206}Pb/^{238}U$ age profiles required rapid cooling through the Pb PRZ (from >650 °C) during the early Jurassic, thus challenging the traditionally-accepted slow-cooling history of the IVZ at rates <5 °C/Myr since ~288 Ma.

Ewing et al. [83] determined U-Pb dates of rutile from granulite facies metapelites from the base of the IVZ (by SIMS) and identified in the scattered $^{206}Pb/^{238}U$ date distributions of their samples two main peaks at ~175 and ~160 Ma. The additional U-Pb rutile data of Smye et al. [89] from the lower crust of the IVZ (average of 180 ± 22 Ma, 2s) are consistent with the previously published data.

Combined, all the U-Pb data from the lower crustal section of the IVZ (spanning paleo-depths from ~34 to 24 km as derived from peak metamorphic P estimates; Figure 4 of Smye et al. [89]) are ~100 Myr younger than the age of the high-T regional metamorphism and testify to cooling of the lowermost portion of the IVZ from temperatures exceeding 600 °C around 180 Ma.

4. Coupled U-Pb Zircon-Rutile Dating Applied to Sediment Provenance in the Eastern Himalayan-Indo-Burman Region

Dating techniques are widely applied to provenance studies in order to discriminate between potential source areas, to track the evolution of river drainage basins, to assess sediment budgets and erosion patterns across orogens and to infer feedback relationships between erosion, tectonics and climate. The Himalayan orogen (together with its sink represented by the deep-sea Bengal Fan) with its scale, ongoing deformation and erosion, is the ideal laboratory for the application of the full range of available thermo- and geo-chronometers (e.g., [101,106,116–123]).

It is only in recent years that U-Pb dating of detrital rutile has been employed in multi-technique provenance studies of Eastern Himalayan- and Indo-Burman- derived sediments [42,84,109–111]. In this section, modern sediment and bedrock detrital rutile U-Pb data from these studies are summarized and compared to zircon data determined on the same samples to show the ability of the coupled U-Pb zircon-rutile provenance proxy of tracking multiple thermal events in the sediment source areas.

4.1. The Tibet-Himalaya-Indo-Burman Region

The Himalayan orogen is the result of ongoing collision between the Indian and Asian plates [124], with onset of the continental collision dated at ca. 59–54 Ma [125,126]. The western and eastern syntaxial orogenic bends of the Himalaya (Figure 5a) manifest the progressive indentation of Indian lithosphere into Asia. The boundary between the Asian and Indian plates is marked by the Indus-Yarlung Tsangpo Suture Zone (Figure 5b). North and south of the suture, respectively, lie the Lhasa Terrane in the Asian plate (intruded by the Jurassic–Paleogene Transhimalayan Andean-type continental arc) and the Tethyan Himalaya (TH, Paleozoic–Eocene sedimentary succession deposited on the northern passive margin of India). The South Tibetan Detachment zone (STD) separates the TH from the Greater

Himalaya (GH, mostly Neoproterozoic metasedimentary rocks at amphibolite to granulite facies). The Main Central Thrust (MCT) separates the latter from the Lesser Himalaya (LH, mostly Precambrian to Paleozoic unmetamorphosed or low-grade Indian crust material). The Main Boundary Thrust (MBT) separates the LH from the foreland basin (Siwalik Group).

The Indo-Burman Ranges (IBR, Figure 5b) is a Cenozoic accretionary prism developed in response to the oblique subduction of the Indian Plate under the Burmese active margin, with Paleogene rocks predominantly derived from the Burmese margin to the east, and Neogene rocks considered to be off−scraped from the Bengal Fan [127–129]. The IBR is bounded to the east by the Central Myanmar Basin (CMB), a predominantly Cenozoic forearc-backarc basin, split by the Western Myanmar Arc (WMA) which is largely buried beneath sedimentary rocks. The CMB is bounded to the east by the Sagaing Fault and the adjacent Mogok Metamorphic Belt to its east (MMB, comprised of low- to high-grade metamorphic rocks, metamorphosed and subsequently exhumed between the Eocene and Early Miocene).

The main drainage of the region is the Himalayan-sourced Ganges-Brahmaputra River system which together with the deep-sea Bengal Fan represents the Earth's largest modern-day source-to-sink sediment-dispersal system, with a drainage basin area of $>2 \times 10^6$ km^2 (Figure 5a) including much of the high-relief Himalaya and the southern Tibetan Plateau ([108] and references therein). In the Eastern Himalayan region, the Brahmaputra originates in Tibet as the Yarlung Tsangpo River, which flows eastwards along the India–Asia suture zone, and crosses the Namche Barwa massif of the eastern Himalayan syntaxis where it bends sharply south. After crossing the Himalaya as the Siang River, it finally flows as the Brahmaputra River to the Bengal plains where it joins the Ganges River before emptying into the Bay of Bengal (Figure 5b). Current erosion rates averaged over the area of the entire Brahmaputra catchment are estimated to be ~2.9 mm/year [130].

4.2. Modern U-Pb Zircon-Rutile Chronology of Eastern Himalayan-Tibet Drainages

The available U-Pb zircon and rutile data of modern river sand samples from the Yarlung Tsangpo-Brahmaputra River and its tributaries draining the Eastern Himalayan region are presented in Figure 6. The data are plotted as cumulative age distribution diagrams [131]. The reader is referred to [42,84] for Concordia diagrams and relative probability-frequency plots of the same data.

The detrital zircon populations of tributaries draining the southern Lhasa Terrane (Lhasa and Niyang Rivers, samples a1 and a4; Figure 6b,c) are dominated by a large proportion of 50–70 Ma zircons derived from the Gangdese Batholith of the Jurassic-Paleogene Transhimalayan Arc (Figure 4 of [42]). The youngest rutile grains in the same samples are 18 and 55 Ma. The Nyiang River is dominated by a 100–200 Ma rutile population, testifying to a cooling event (possibly following a metamorphic overprint) occurred within the southeastern Lhasa basement. Zircon and rutile of Cretaceous–Paleogene age appear to have been derived from originally distinct sources in both samples since rutile grains are systematically older than zircon grains within this age interval. A prominent 500–600 Ma rutile population is identified in the Lhasa tributary (a4) and also in the main trunk of the Yarlung Tsangpo upstream of the syntaxis at two locations >200 km apart from each other (Y and W in Figure 6a,n), supporting the occurrence of a major source with this cooling age signature in the southern Lhasa Terrane. A rutile population of similar age (500–550 Ma) occurs in the modern Dhansiri River that drains the IBR (sample b7; Figure 6m). The Yarlung Tsangpo rutile samples upstream of the syntaxis (Y and W; youngest grains respectively ~12 and 8 Ma) exhibit two strikingly similar patterns also in terms of the <50 Ma population, with 10–20 Ma rutiles possibly derived from Himalayan sources south of the suture or from Lhasa magmatism.

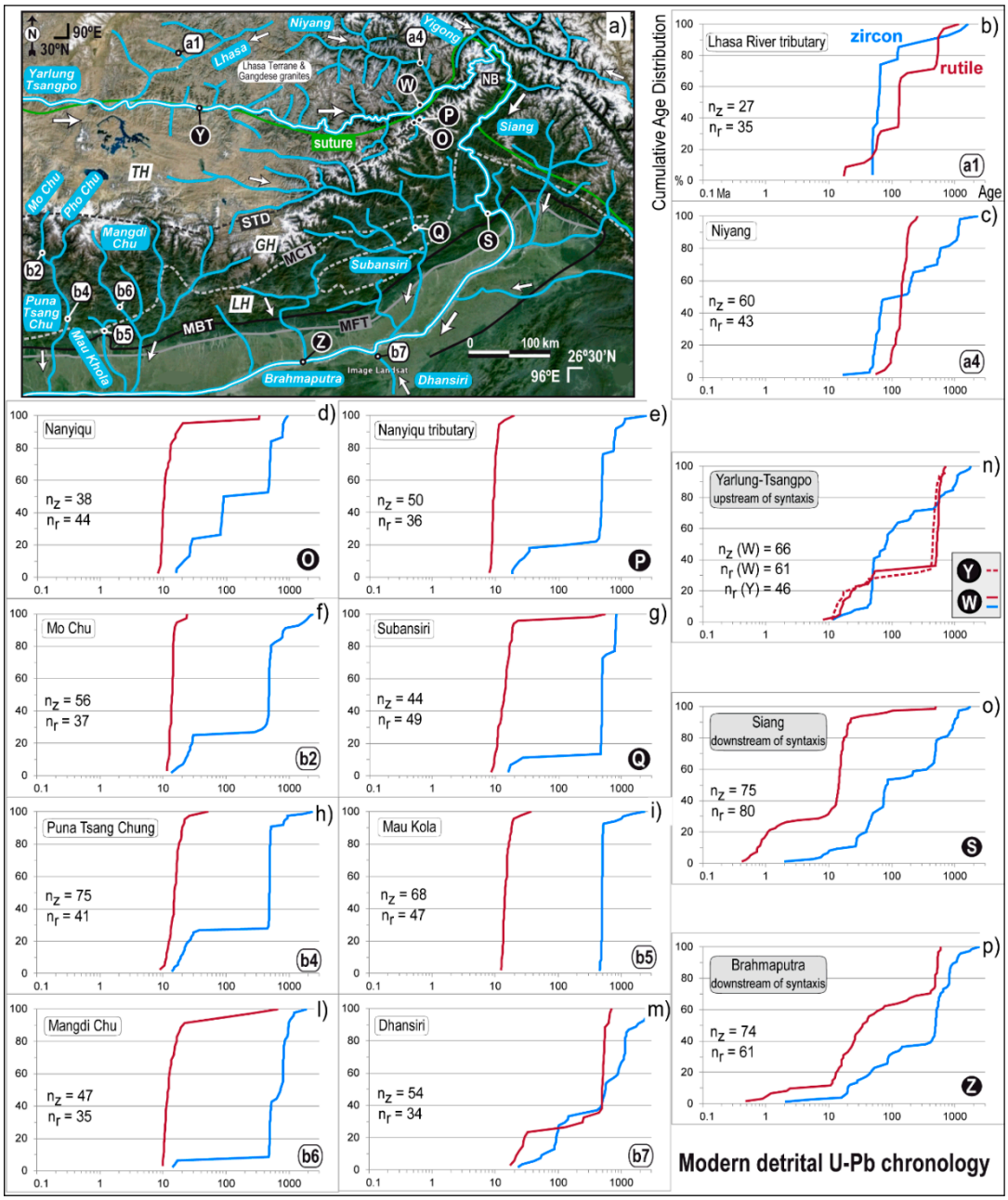

Figure 6. (**a**) Map showing the modern Yarlung Tsangpo–Brahmaputra drainage network in the Eastern Himalaya superimposed on a Google Earth Landsat image. Locations of modern river sand samples for which both U-Pb zircon and rutile data have been collected are shown. White arrows indicate river flow direction. See text for abbreviations of Himalayan lithotectonic units (TH, GH, and LH) and their bounding faults (STD, MCT, MBT, and MFT). NB: Namche Barwa massif in the eastern Himalayan syntaxis. Modified from [84]. (**b**–**p**) U-Pb zircon and rutile cumulative age distribution plots of modern river sand samples from the Yarlung Tsangpo-Brahmaputra main trunk (upstream, samples W and Y and downstream of the eastern syntaxis, samples S and Z) and its tributaries draining: the Lhasa block of the Asian plate (a1 and a4); the southwestern flank of the syntaxial antiform (O and P); the Greater Himalaya (Q, b2, b4, b5, and b6); and the Indo-Burman Ranges (b7). U-Pb data from [42,59,84]. For each sample nz and nr, respectively, indicate the number of zircon and rutile dates plotted in the diagram after rejection of discordant data.

All tributaries draining the Himalayan slopes south of the India-Asia suture (i.e., draining TH and GH rocks [123]) exhibit a ~500 Ma zircon age population (Figure 6d–l) that characterizes Indian-derived sediments and corresponds to the intrusion of late "Pan-African" granites [132]. In these samples, the 50–70 Ma population that is distinctive of the Gangdese Batholith in the Asian plate is lacking and ~15–30 Ma zircon rims (up to 30% of the sample) testify to Cenozoic Himalayan metamorphism affecting GH [84]. Rutile in the same samples is dominated by late Miocene ages (youngest grains: ~9–13 Ma), with some older components as old as Paleozoic probably derived from Tethyan sedimentary sources. Such ~9–15 Ma rutile age signature testifies to the exhumation of GH following Himalayan metamorphism and is minor in the Yarlung Tsangpo upstream of the syntaxis but prominent in the Siang and Brahmaputra at locations S and Z (Figure 6a,o,p) receiving the contribution of tributaries draining the southern slopes of the Himalayan orogen dominated by GH. As previously mentioned (Section 3.2), Warren et al. [112] suggested that 10–11 Ma rutiles from granulite and amphibolite facies GH rocks constrain the timing of rapid cooling from peak T conditions of ~800 °C at 14 Ma and ~650 °C at 12 Ma in the granulites and amphibolites, respectively.

Both S and Z samples exhibit a very young (approximately <4 Ma) rutile age component. which is distinctive of detritus eroded from the eastern syntaxis (cf. the ~1.4 Ma bedrock rutile from the Namche Barwa massif at the core of the syntaxial antiform, Section 3.2; Figure 7). The 50–70 Ma Gangdese Batholith zircon source and the "Pan-African" (~500 Ma) Indian component are also recognized in the two Brahmaputra samples S and Z. The comparison of samples W, S and Z constrains the evolution of the downstream signature along the main trunk of the Yarlung Tsangpo-Brahmaputra, with enhancement of the GH signature in sample S and the appearance of a ~30% syntaxial component (<3 Ma). The latter, although reduced to ~10%, is still preserved in sample Z several 100s km downstream.

These modern detrital data highlight the ability of the U-Pb rutile chronometer in tracking sources at the regional scale, such as the 500–600 Ma source in the Lhasa Terrane, the 9–15 Ma Greater Himalaya source and the <3 Ma eastern syntaxis source. The cooling age signature of each source is readily identifiable and distinct from the zircon U-Pb signature in the same sample. It is important to bear in mind that in general this could reflect, in addition to the different Pb retentivity behavior of zircon vs. rutile in the same rock source (as pointed out for bedrock samples, see Section 3.2 and Figure 4), also derivation of zircon and rutile grains in each sample from distinct sources that do not bear both minerals as accessory phases (as it is most likely the case of samples a1 and a4, Figure 6b,c). In this latter sense, coupling the two chronometers enhances the possibility of identifying a wider range of sources hence more accurately determining the provenance of the sediment.

In Figure 7, composite samples representing the modern detrital chronology of the entire Brahmaputra drainage basin (main river trunk and tributaries) are compared to the typical age signature of the main bedrock sources known in the Himalayan-Indo-Burman region. In addition to U-Pb zircon and rutile data, Ar-Ar white mica data are plotted (see figure caption for data sources). White mica is a lower-T thermochronometer, which is retentive of radiogenic Ar below ~400 °C ([133] and references therein). The overall younger age signature of detrital white mica from the Brahmaputra drainage basin (Figure 7a) primarily reflects the different response to cooling of the Ar-Ar chronometer compared to rutile and highlights its complementarity in tracking the same (or distinct) tectono-thermal events in the bedrock sources. As mentioned in Section 3.2, one of the best examples of how various geo- and thermo-chronometers altogether sensitive to T in excess of 800 °C down to approximately <100 °C respond differently to the same thermal event(s) is provided by the rapidly exhuming core of the eastern Himalayan syntaxis (ES in Figure 7b; see summary Figure 2 of [84], [107] and references therein). Strikingly, the unique isotopic signature of the ES source, comprising an area of only ca. 40 km by 40 km, i.e., <0.5% of the entire Brahmaputra drainage basin (~580,000 km^2 [130]) is preserved even in the composite samples of Figure 7.

The many published multi-chronometer provenance studies carried out in the Himalayan-Indo-Burman region and other regions similarly characterized by a complex orogenic evolution encourage the combined application of multiple chronometers to resolve the full range of

tectono-thermal events that affected the source rocks (e.g., [134]). Detrital U-Pb thermochronology can certainly play a key role in this context, as shown by the case studies presented in the next section.

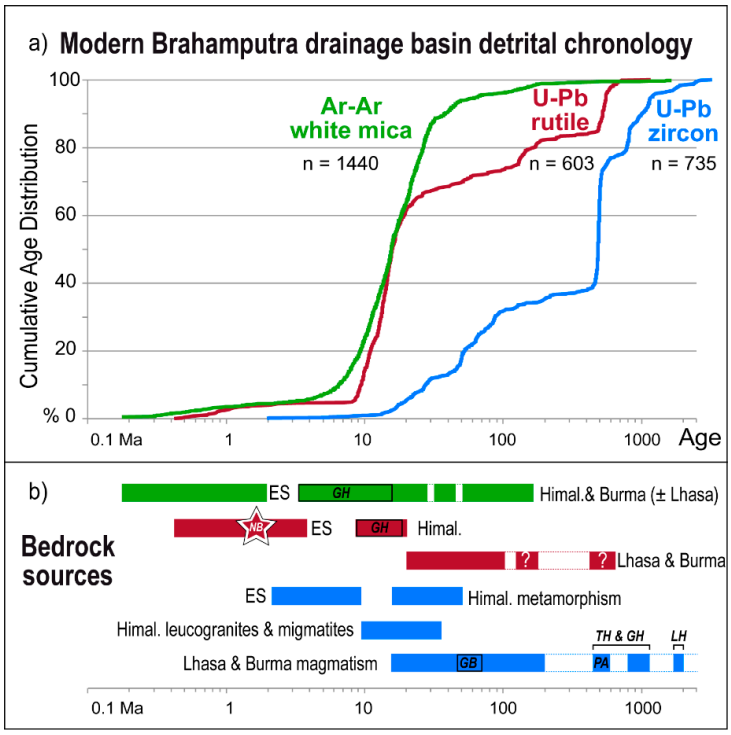

Figure 7. Summary of detrital chronology data from the modern Brahmaputra drainage (main trunk and tributaries) and comparison to bedrock sources. (**a**) Cumulative age distribution plots of Brahmaputra composite samples (Ar-Ar white mica data of 22 samples from [84,135–137]; U-Pb rutile and zircon data: same 14 samples plotted in Figure 6); n indicates the total number of analyses per sample. (**b**) Typical age range of the main bedrock sources from the Eastern Himalayan-Indo-Burman region. Ages of approximately <10 (zircon), 4 (rutile) and 2 Ma (white mica) are unique to the core of the eastern syntaxial antiform (ES) [84,106,137]. Star labeled NB indicates the ~1.4 Ma rutile from the Namche Barwa massif [84]. The Himalayan metamorphic peak is identified by ~15–40 Ma zircons [138], typically occurring as overgrowths on older zircons [42]. Circa 9–15 Ma rutiles and white micas in the same age range (but also as young as 3–6 Ma) likely testify to cooling following exhumation of Greater Himalayan rocks (GH) [84,137]. White micas in the range 4–20 Ma can also be contributed from the Asian plate (Lhasa) or Burma/Indo-Burman sources, although the latter show a large majority of ages > 20 Ma ([137] and references therein). Both the Asian and Burma plates show evidence for igneous sources as young as 10–15 Ma [139–145]; note the 50–70 Ma detrital zircon population of the Brahmaputra sourced by the Gangdese Batholith (GB) [42]. Prominent pre-Himalayan rutile sources to the Brahmaputra detritus (e.g. in the range 100–200 Ma) are yet to be identified due to the lack of U-Pb rutile bedrock data in this region. Interestingly, 400–600 Ma rutile occurs in modern detritus eroded from both Lhasa and Burma. Late Pan-African (PA, ~500 Ma) and older detrital zircon populations can derive from Himalayan (i.e., Indian-derived sediments), Asian (Lhasa) or Burma bedrock sources. Erosion of Greater and Tethyan Himalayan (TH) units typically produces detrital zircon age distributions with main peaks at ~0.5 and 0.8–1.2 Ga, while in Lesser Himalayan (LH) detritus the dominant U–Pb zircon age range is 1.7–2.0 Ga ([119,123] and references therein).

4.3. Coupled U-Pb Zircon-Rutile Chronology Applied to Cenozoic Himalayan-Indo-Burman Sediment Repositories

This section presents examples of applications of the coupled zircon-rutile U-Pb provenance proxy in multi-technique detrital studies aimed at unravelling tectonic-erosion coupling, drainage and orogen evolution in the Himalayan-Tibet and Indo-Burman regions. The emphasis here is on U-Pb

chronology of zircon and rutile, hence the other thermo-chronometers employed in the cited studies (e.g., zircon fission track, Ar-Ar white mica, U-Pb apatite dating) are omitted. Additionally, only a few key samples (out of the many investigated by the authors) are plotted in the following figures to highlight the complementary significance of the zircon and rutile U-Pb chronometers employed as provenance proxies. The reader is referred to the original publications for full context and results, as well as detailed references for the study areas, which is beyond the aims of this work to present in detail here.

Bracciali et al. [42] addressed the long-debated occurrence and timing of river capture of the Yarlung Tsangpo by the Brahmaputra River by investigating the paleo-Brahmaputra deposits in the Surma Basin. The Surma Basin, a sub-basin of the Bengal Basin in north-eastern Bangladesh (location 1 in Figure 5b), is comprised of a 16 km thick Eocene–Pleistocene sedimentary package of limestone and clastic rocks. Most of the Bengal Basin fill consists of sediments fluvially transported by the Ganges and Brahmaputra and their ancestral river systems. Bracciali and co-authors documented the arrival of Cretaceous–Paleogene zircons in Early Miocene sediments of the paleo-Brahmaputra River (sample BA03-13A in Figure 8, corresponding to sample 8 in Figure 2 of [42]). This was interpreted as first influx of detritus from the Transhimalayan arc of the Asian plate (cf. the modern detrital zircon signature of rivers draining the southern Lhasa terrane of the Asian plate, Figure 6b,c) transported by the Yarlung Tsangpo following its capture by the Brahmaputra. Prior to capture, the predominantly Precambrian–Paleozoic U-Pb zircon signature in the older Surma Basin sedimentary record (not shown in Figure 8) indicated that only the Indian plate was drained. Contemporaneous with Transhimalayan influx, the Surma Basin recorded progressively increased erosion of the metamorphosed core of the Himalyan orogen as testified by increasing proportion and younging upsection of Cenozoic detrital rutiles and zircons (e.g., samples LBA-5a and -15a in Figure 8, corresponding to samples 24 and 34 in [42]).

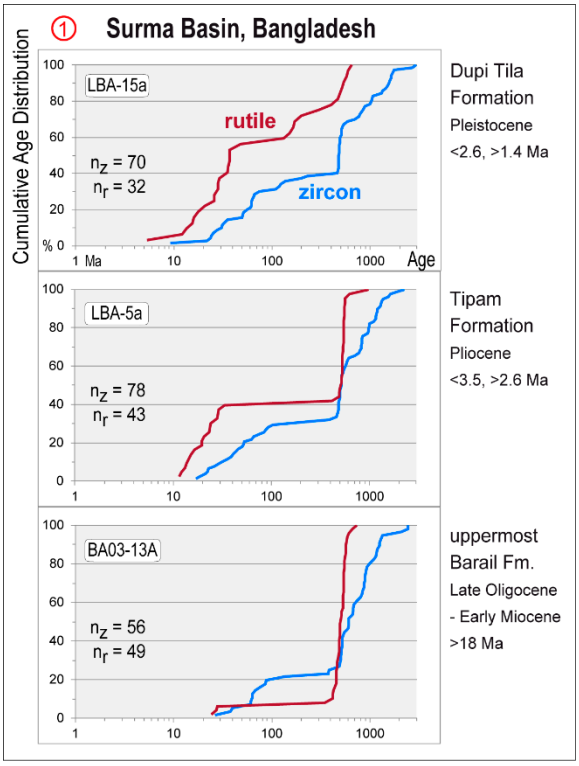

Figure 8. Detrital U-Pb zircon and rutile data of sandstone samples from the Surma Basin (Bangladesh) plotted as cumulative age distribution diagrams. The red circled number indicates the sample location in Figure 5. Sample labels and stratigraphic age constraints are also indicated. Data from [42].

Govin et al. [109] used the sedimentary record of the Himalayan foreland basin north of the Shillong Plateau to test a potential diversion of the paleo-Brahmaputra river course (and its timing) as a consequence of the topographic growth of the Shillong Plateau (an uplifted block of Precambrian Indian plate basement, partially overlain by Cretaceous and Cenozoic sediments, Figure 5b). The study reported detrital zircon U-Pb data from the Dungsam Chu stratigraphic section (Siwalik Group) in Bhutan, located directly north of the Shillong Plateau (location 2 in Figure 5b).

The first appearance in a Pliocene sandstone sample (SJ8, Figure 9) of Cretaceous–Cenozoic grains derived from the Transhimalaya (absent in stratigraphically older samples and present in samples younger than SJ8, not shown in Figure 9) was interpreted to show redirection of the Brahmaputra River north and west of the plateau as a consequence of the surface uplift of the plateau. Rutile U-Pb dating of the same sample returned ~25% of the grains <9 Ma interpreted as derived from the erosion of the eastern syntaxis, hence supporting the interpretation of the Brahmaputra flowing in the Himalayan foreland at Dungsam Chu by ~5 Ma, the timing of the deposition of sample SJ8.

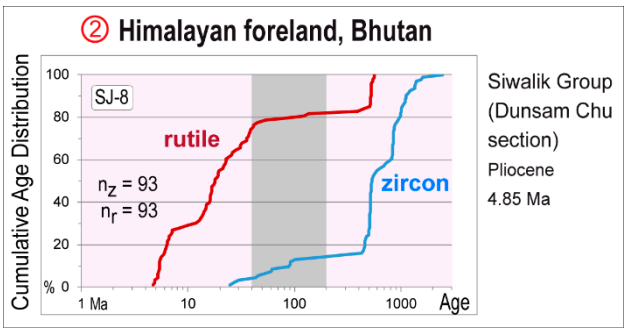

Figure 9. Detrital U-Pb zircon and rutile data of one sandstone sample from the foreland Himalayan deposits (Siwalik Group, Dungsam Chu section, Bhutan, location indicated by the red circled number in Figure 5) plotted as cumulative age distribution diagrams. Sample label and stratigraphic age constraints are also indicated. Gray band shows the age range characteristic of Transhimalayan Arc sources in the southern Lhasa block. Data from [109].

Zhang et al. [110] U-Pb dated drillcore and outcrop sandstone samples from the Central Myanmar Basin (locations 3 and 4 in Figure 5b) to test a potential connection between the Yarlung Tsangpo and the Irrawaddy River (which today flows through the CMB) prior to the Early Miocene, since when the Yarlung Tsangpo is known to have flown into the Bengal Basin following capture by the Brahmaputra [42].

All detrital zircon samples in Zhang et al.'s study are dominated by Mesozoic–Cenozoic grains, with a ~80–100 Ma population prominent in Paleocene−Eocene samples (e.g., samples Y3-81 and MY16-64A in Figure 10), less prominent in Oligocene samples and subordinate by Miocene times when a ~50–75 Ma population becomes dominant (e.g., samples Y3-13 and MY16-56A in Figure 10).

Paleocene−Eocene detrital rutile samples yield main populations between ~400 and 600 Ma, presumably derived from the Burmese basement. A modest contribution of rutile grains between 40 and 80 Ma is recorded in the middle Oligocene surface outcrop samples, with a ~40 Ma population dominating by the time of deposition of the subsurface upper Oligocene sample and in the rest of the overlying succession. These ~40 Ma rutiles are interpreted as derived from the erosion of the exhumed Mogok Metamorphic Belt to the east of the Sagaing fault. A positive εHf signature determined for the Mesozoic–Cenozoic detrital zircons in the rocks of Eocene age and older is interpreted to be derived from a local igneous source, likely the Western Myanmar Arc. In contrast, Miocene samples include a substantial additional population of grains with negative εHf values, compatible with derivation from the Eastern Batholiths (typically $\varepsilon Hf < 0$) rather than from the Gangdese Batholith of the Transhimalaya (typically $\varepsilon Hf > 0$). Such a change in provenance between the Eocene and the Miocene was interpreted in terms of the MMB and Eastern Batholiths becoming a significant new source region providing

detritus to the CMB through establishment of a paleo–Irrawaddy trunk river by middle Oligocene times, without requiring a paleo Yarlung Tsangpo-Irrawaddy connection (Figure 21 of Zhang et al. [110]).

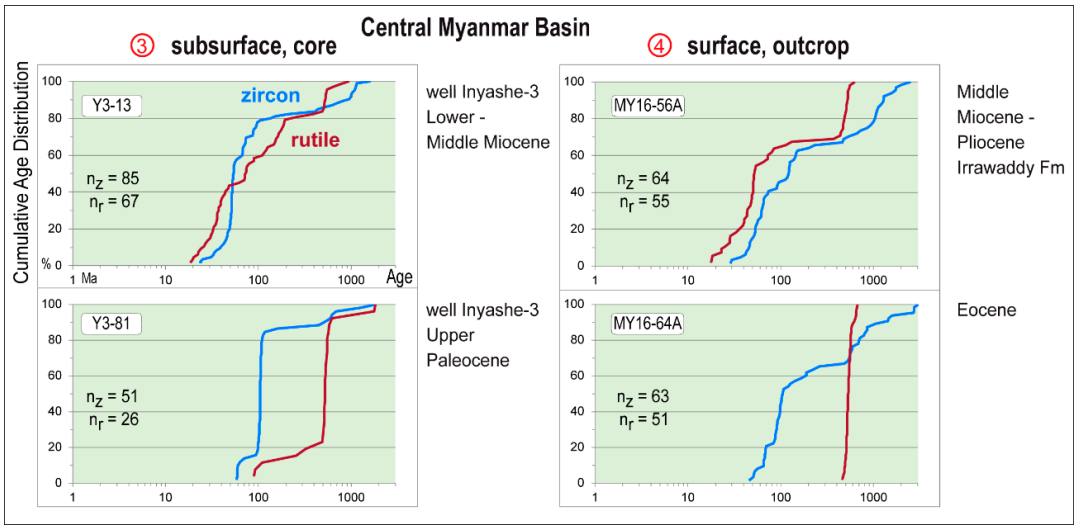

Figure 10. Detrital U-Pb zircon and rutile data of sandstone samples from the Central Myanmar Basin plotted as cumulative age distribution diagrams. The red circled numbers indicate the sample locations in Figure 5. Sample labels and stratigraphic age constraints are also indicated. Data from [110].

In 2015, the IODP expedition 354 drilled seven sites along a proximal (°8N) east-west transect in the Bay of Bengal (Figure 5a) covering the Late Paleogene to present sedimentation of the Bengal Fan [146]. The Bengal Fan covers the entire floor of the Bay of Bengal, from the continental margins of India and Bangladesh to the sediment-filled Sunda Trench off Myanmar and the Andaman Islands. An estimated 30% of the total modern sediment load feeding the delta plain in India and Bangladesh is derived from the Ganges and up to 70% from the Brahmaputra [108].

Strikingly, after up to 2500 km of fluvial transport and >1400 km of transport by turbidity currents, the U-Pb record recovered from Miocene to middle Pleistocene Bengal Fan turbidites [108] faithfully represents Himalayan sources (Figure 11). The main zircon populations include the ~ 500 Ma peak typical of GH and TH as well as older zircons (Figure 11; cf. the Brahmaputra signature in Figures 6 and 7). Mesozoic and Cenozoic populations with broad peaks at ca. 50–60 and 110–130 Ma (consistent with derivation from the Transhimalaya of the Lhasa Terrane) increase up-section and include a minor population of ~15–40 Ma zircon grains likely testifying to the Himalayan high grade metamorphism and leucogranites or Lhasa magmatism ([108]; cf. Figure 7b). Importantly, in the Bengal Fan, Transhimalayan zircons have been found from the base of the fan, dated at 18 Ma at that location [108], consistent with an established Yarlung Tsangpo–Brahmaputra connection by that time [42].

Similar to the zircon data, the rutile U-Pb data in Bengal Fan sediments younger than 10 Ma [111] track the erosion of Himalayan sources, such as the ~500–600 Ma source (identified in modern detritus eroded from the Lhasa terrane, Figure 6b, but also present in the modern Dhansiri River draining the IBR, Figure 6m) or the 10–15 Ma GH source (Figures 6d–l and 7).

The first appearance of lag times (i.e., the difference between the mineral cooling age and the host sediment depositional age) of <1 Myr occurs in a sample with depositional age between 3.76 and 3.47 Ma. The next analyzed sample stratigraphically below, with a depositional age between 4.50 and 5.59 Ma, exhibits lag times of >6 Myr. The short (<1 Myr) lag times (also observed in zircon fission track data) continue to be recorded upward in the core to the youngest sediments analyzed, deposited at <1 Ma (Figure 11, cf. the modern Siang signature in Figure 6o). Najman et al. [111] interpreted the earliest record of short lag times to represent the onset of extremely rapid exhumation of the Eastern Himalayan syntaxial massif starting sometime between 5.59 and 3.47 Ma.

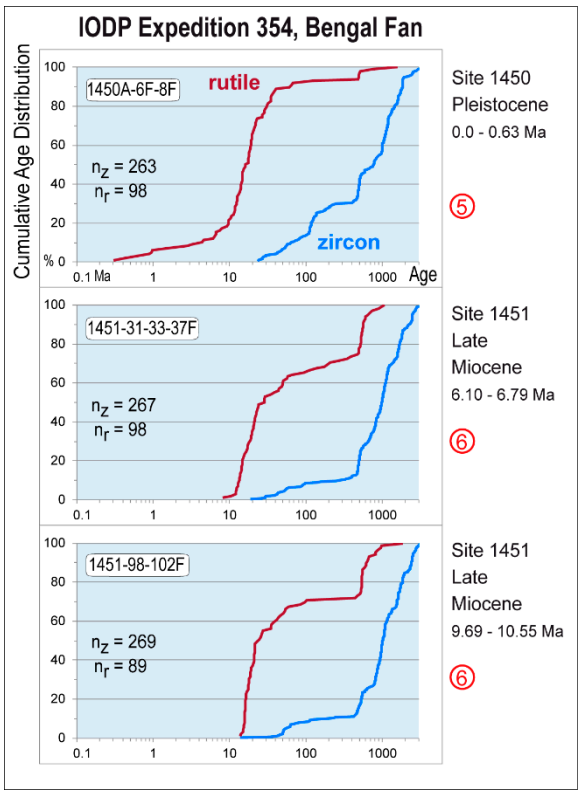

Figure 11. Detrital U-Pb zircon and rutile data of sandstone samples from the Bengal Fan plotted as cumulative age distribution diagrams. The red circled numbers indicate the site locations in Figure 5a. Sample labels and stratigraphic age constraints are also indicated. U-Pb data from [101,104]

5. Conclusions and Future Directions

The availability of good quality rutile reference materials and the development of strategies to address the generally lower average U concentrations in rutile compared to zircon (hence, measurable radiogenic Pb) and to correct—when necessary—rutile grains for common Pb encourage U-Pb dating of rutile by LA ICP-MS.

The application of this technique benefits from a better understanding, developed in the last decade, of the natural processes affecting the U-Pb systematics of rutile, primarily thermally-activated Pb volume diffusion but also re-crystallization and secondary growth (during metamorphism) and/or the presence of grain boundary fluids of variable chemical composition.

The chemical and mechanical robustness of rutile and zircon and their occurrence as accessory phases in a wide range of crustal rocks makes both minerals ideal provenance proxies. The first applications of rutile U-Pb chronology coupled to zircon U-Pb chronology (and other thermo- and geochronometers) to provenance studies in the Eastern Himalayan-Indo-Burman region [42,84,109–111] have proven the effectiveness of the coupled provenance proxy in tracking tectono-thermal events in the source areas across a wide range of temperatures, from medium- to high-T igneous and metamorphic crystallization to cooling through ~600 °C. This approach is key to characterize detritus sourced from areas with complex poly-phase metamorphic histories such as collisional orogens.

Another thermochronometer in which volume diffusion of Pb occurs at temperatures relevant to the evolution of the middle and lower crust is apatite, which tracks cooling through ~375–550 °C [147]. However, elevated common Pb (which is typically divalent [148]) is observed in apatite compared to rutile, likely due to preferential substitution into the apatite crystal lattice of common Pb^{2+} for Ca^{2+}, with radiogenic Pb (typically tetravalent) presumably hosted interstitially or in defects [149], hence more subject to diffusion out of the lattice. As pointed out by Najman et al. [111], the high common to radiogenic Pb ratio in apatite results in high age uncertainty especially in young grains

(e.g., absolute age uncertainty up to 50% for 10–100 Ma apatites). This is interpreted to be the most likely cause for apatite grains with short (<1 Myr) lag times not being observed in the Bengal Fan samples or in syntaxially-derived modern river sediment, in contrast to rutile. Hence, the apatite U-Pb thermochronometer is suited to record Himalayan sources but not syntaxial exhumation [111].

A thorough characterization of the U-Pb rutile signature of bedrock sources in the Tibet-Himalaya-Burma region is currently limited and primarily based on U-Pb dating of modern river sands. An effort in this direction from the U-Pb LA ICP-MS community is highly desirable and will certainly facilitate the interpretation of provenance data in the future.

Finally, the current level of precision achieved by LA ICP-MS rutile dating is limited by the natural scatter in the isotopic ratios of the reference material used for normalization purposes, and by the accuracy and precision to which such material is known. Further investigation of the pattern and causes for the natural U/Pb variability observed in the rutiles currently used as primary reference materials and the identification and age characterization (by ID-TIMS) of the most isotopically homogeneous domains within these rutiles (or new candidate reference materials) could result in the refinement of the isotopic values used for normalization of the LA ICP-MS data, in a similar way to that which has been done in recent years for zircon reference materials (e.g., [14]). Consequently, this would improve the precision hence the quality of the sample U-Pb data, which in turn would allow deriving more robust time constraints on geological events and processes.

Funding: Stellenbosch University funded 50% of the journal article processing charges through the Library's Open Access Publication Fund.

Acknowledgments: I warmly thank: Randy Parrish for steering our early work on U-Pb dating of rutile at the NERC Isotope Geosciences Laboratory (now Geochronology and Tracers Facility, GTF), British Geological Survey (BGS); Matt Horstwood (GTF-BGS) for discussion on all aspects of LA ICP-MS isotopic analysis aimed at generating optimal quality, geologically meaningful data and for his comments on an advanced draft of the manuscript; and Yani Najman (Lancaster University) for sharing enthusiasm on the application of the detrital zircon- rutile U-Pb chronometer to address complex erosion-tectonic questions in the Himalayan context. This manuscript benefited from the comments of three anonymous reviewers and is published with the permission of the Executive Director of the BGS.

Conflicts of Interest: The author declares no conflict of interest.

References

1. Schoene, B. U-Th-Pb Geochronology. In *Treatise on Geochemistry*, 2nd ed.; Elsevier: Amsterdam, The Netherlands, 2013; pp. 341–378. ISBN 9780080983004.
2. Parrish, R.R.; Noble, S.R. Zircon U-Th-Pb geochronology by isotope dilution—Thermal ionization mass spectrometry (ID-TIMS). *Rev. Mineral. Geochem.* **2003**, *53*, 183–213. [CrossRef]
3. Mattinson, J.M. Zircon U-Pb chemical abrasion ("CA-TIMS") method: Combined annealing and multi-step partial dissolution analysis for improved precision and accuracy of zircon ages. *Chem. Geol.* **2005**, *220*, 47–66. [CrossRef]
4. Ireland, T.R.; Williams, I.S. Considerations in Zircon Geochronology by SIMS. *Rev. Mineral. Geochem.* **2003**, *53*, 215–241. [CrossRef]
5. Košler, J.; Sylvester, P.J. Present Trends and the Future of Zircon in Geochronology: Laser Ablation ICPMS. *Rev. Mineral. Geochem.* **2003**, *53*, 243–275. [CrossRef]
6. Schaltegger, U.; Schmitt, A.K.; Horstwood, M.S.A. U-Th-Pb zircon geochronology by ID-TIMS, SIMS, and laser ablation ICP-MS: Recipes, interpretations, and opportunities. *Chem. Geol.* **2015**, *402*, 89–110. [CrossRef]
7. Schoene, B.; Condon, D.J.; Morgan, L.; McLean, N. Precision and Accuracy in Geochronology. *Elements* **2013**, *9*, 19–24. [CrossRef]
8. Sylvester, P.J.; Jackson, S.E. A Brief History of Laser Ablation Inductively Coupled Plasma Mass Spectrometry (LA–ICP–MS). *Elements* **2016**, *12*, 307–310. [CrossRef]
9. Günther, D.; Koch, J. Formation of aerosols generated by laser ablation and thir impact on elemental fractionation in LA-ICP-MS. In *Laser Ablation ICP–MS in the Earth Sciences: Current Practices and Outstanding Issues*; Mineralogical Association of Canada: Quebec City, QC, USA, 2008; pp. 19–34. ISBN 0921294492.

10. Paton, C.; Woodhead, J.D.; Hellstrom, J.C.; Hergt, J.M.; Greig, A.; Maas, R. Improved laser ablation U-Pb zircon geochronology through robust downhole fractionation correction. *Geochem. Geophys. Geosyst.* **2010**, *11*. [CrossRef]
11. Ver Hoeve, T.J.; Scoates, J.S.; Wall, C.J.; Weis, D.; Amini, M. Evaluating downhole fractionation corrections in LA-ICP-MS U-Pb zircon geochronology. *Chem. Geol.* **2018**, *483*, 201–217. [CrossRef]
12. Košler, J.; Sláma, J.; Belousova, E.; Corfu, F.; Gehrels, G.E.; Gerdes, A.; Horstwood, M.S.A.; Sircombe, K.N.; Sylvester, P.J.; Tiepolo, M.; et al. U-Pb Detrital Zircon Analysis – Results of an Inter-laboratory Comparison. *Geostand. Geoanalytical Res.* **2013**, *37*, 243–259. [CrossRef]
13. Woodhead, J.D.; Horstwood, M.S.A.; Cottle, J.M. Advances in Isotope Ratio Determination by LA–ICP–MS. *Elements* **2016**, *12*, 317–322. [CrossRef]
14. Horstwood, M.S.A.; Košler, J.; Gehrels, G.; Jackson, S.E.; McLean, N.M.; Paton, C.; Pearson, N.J.; Sircombe, K.; Sylvester, P.; Vermeesch, P.; et al. Community-Derived Standards for LA-ICP-MS U-(Th-)Pb Geochronology – Uncertainty Propagation, Age Interpretation and Data Reporting. *Geostand. Geoanalytical Res.* **2016**, *40*, 311–332. [CrossRef]
15. Harley, S.L.; Kelly, N.M. Zircon Tiny but Timely. *Elements* **2007**, *3*, 13–18. [CrossRef]
16. Hoskin, P.W.O.; Schaltegger, U. The composition of zircon and igneous and metamorphic petrogenesis. *Rev. Mineral. Geochem.* **2003**, *53*, 27–62. [CrossRef]
17. Hanchar, J.M.; Miller, C.F. Zircon zonation patterns as revealed by cathodoluminescence and backscattered electron images: Implications for interpretation of complex crustal histories. *Chem. Geol.* **1993**, *110*, 1–13. [CrossRef]
18. Kempe, U.; Gruner, T.; Nasdala, L.; Wolf, D. Relevance of Cathodoluminescence for the Interpretation of U-Pb Zircon Ages, with an Example of an Application to a Study of Zircons from the Saxonian Granulite Complex, Germany BT - Cathodoluminescence in Geosciences. In *Cathodoluminescence in Geosciences*; Pagel, M., Barbin, V., Blanc, P., Ohnenstetter, D., Eds.; Springer: Berlin/Heidelberg, Germany, 2000; pp. 415–455. ISBN 978-3-662-04086-7.
19. Rubatto, D.; Gebauer, D. Use of Cathodoluminescence for U-Pb Zircon Dating by Ion Microprobe: Some Examples from the Western Alps. In *Cathodoluminescence in Geosciences*; Pagel, M., Barbin, V., Blanc, P., Ohnenstetter, D., Eds.; Springer: Berlin/Heidelberg, Germany, 2000; pp. 373–400. ISBN 978-3-662-04086-7.
20. Corfu, F.; Hanchar, J.M.; Hoskin, P.W.O.; Kinny, P. Atlas of Zircon Textures. *Rev. Mineral. Geochem.* **2003**, *53*, 469–500. [CrossRef]
21. Feng, R.; Machado, N.; Ludden, J. Lead geochronology of zircon by LaserProbe-inductively coupled plasma mass spectrometry (LP-ICPMS). *Geochim. Cosmochim. Acta* **1993**, *57*, 3479–3486. [CrossRef]
22. Fryer, B.J.; Jackson, S.E.; Longerich, H.P. The application of laser ablation microprobe-inductively coupled plasma-mass spectrometry (LAM-ICP-MS) to in situ (U)Pb geochronology. *Chem. Geol.* **1993**, *109*, 1–8. [CrossRef]
23. Hirata, T.; Nesbitt, R.W. U-Pb isotope geochronology of zircon: evaluation of the laser probe-inductively coupled plasma mass spectrometry technique. *Geochim. Cosmochim. Acta* **1995**, *59*, 2491–2500. [CrossRef]
24. Engi, M.; Lanari, P.; Kohn, M.J. Significant Ages—An Introduction to Petrochronology. *Rev. Mineral. Geochem.* **2017**, *83*, 1–12. [CrossRef]
25. Kylander-Clark, A.R.C.; Hacker, B.R.; Cottle, J.M. Laser-ablation split-stream ICP petrochronology. *Chem. Geol.* **2013**, *345*, 99–112. [CrossRef]
26. Meinhold, G. Rutile and its applications in earth sciences. *Earth-Sci. Rev.* **2010**, *102*, 1–28. [CrossRef]
27. Rudnick, R.L.; Barth, M.; Horn, I.; McDonough, W.F. Rutile-Bearing Refractory Eclogites: Missing Link Between Continents and Depleted Mantle. *Science (80-.)* **2000**, *287*, 278–281. [CrossRef] [PubMed]
28. Zack, T.; Stockli, D.F.; Luvizotto, G.L.; Barth, M.G.; Belousova, E.; Wolfe, M.R.; Hinton, R.W. In situ U–Pb rutile dating by LA-ICP-MS: 208Pb correction and prospects for geological applications. *Contrib. Mineral. Petrol.* **2011**, *162*, 515–530. [CrossRef]
29. Zack, T.; Kooijman, E. Petrology and Geochronology of Rutile. *Rev. Mineral. Geochem.* **2017**, *83*, 443–467. [CrossRef]
30. Zack, T.; Moraes, R.; Kronz, A. Temperature dependence of Zr in rutile: empirical calibration of a rutile thermometer. *Contrib. Mineral. Petrol.* **2004**, *148*, 471–488. [CrossRef]
31. Watson, E.B.; Wark, D.A.; Thomas, J.B. Crystallization thermometers for zircon and rutile. *Contrib. Mineral. Petrol.* **2006**, *151*, 413. [CrossRef]

32. Ferry, J.M.; Watson, E.B. New thermodynamic models and revised calibrations for the Ti-in-zircon and Zr-in-rutile thermometers. *Contrib. Mineral. Petrol.* **2007**, *154*, 429–437. [CrossRef]
33. Tomkins, H.S.; Powell, R.; Ellis, D.J. The pressure dependence of the zirconium-in-rutile thermometer. *J. Metamorph. Geol.* **2007**, *25*, 703–713. [CrossRef]
34. Watson, E.B.; Harrison, T.M. Zircon Thermometer Reveals Minimum Melting Conditions on Earliest Earth. *Science (80-.)* **2005**, *308*, 841–844. [CrossRef]
35. Kooijman, E.; Smit, M.A.; Mezger, K.; Berndt, J. Trace element systematics in granulite facies rutile: implications for Zr geothermometry and provenance studies. *J. Metamorph. Geol.* **2012**, *30*, 397–412. [CrossRef]
36. Blackburn, T.; Shimizu, N.; Bowring, S.A.; Schoene, B.; Mahan, K.H. Zirconium in rutile speedometry: New constraints on lower crustal cooling rates and residence temperatures. *Earth Planet. Sci. Lett.* **2012**, *317–318*, 231–240. [CrossRef]
37. Siégel, C.; Bryan, S.E.; Allen, C.M.; Gust, D.A. Use and abuse of zircon-based thermometers: A critical review and a recommended approach to identify antecrystic zircons. *Earth-Sci. Rev.* **2018**, *176*, 87–116. [CrossRef]
38. Cruz-Uribe, A.M.; Feineman, M.D.; Zack, T.; Jacob, D.E. Assessing trace element (dis)equilibrium and the application of single element thermometers in metamorphic rocks. *Lithos* **2018**, *314–315*, 1–15. [CrossRef]
39. Andò, S.; Garzanti, E.; Padoan, M.; Limonta, M. Corrosion of heavy minerals during weathering and diagenesis: A catalog for optical analysis. *Sediment. Geol.* **2012**, *280*, 165–178. [CrossRef]
40. Deer, W.A.; Howie, R.A.; Zussman, J. *An Introduction to the Rock-Forming Minerals*; Mineralogical Society of Great Britain and Ireland: London, UK, 2013; ISBN 10 9780903056274; ISBN 13 9780903056434.
41. Axelsson, E.; Pape, J.; Berndt, J.; Corfu, F.; Mezger, K.; Raith, M.M. Rutile R632—A New Natural Reference Material for U-Pb and Zr Determination. *Geostand. Geoanalytical Res.* **2018**, *42*, 319–338. [CrossRef]
42. Bracciali, L.; Najman, Y.; Parrish, R.R.; Akhter, S.H.; Millar, I. The Brahmaputra tale of tectonics and erosion: Early Miocene river capture in the Eastern Himalaya. *Earth Planet. Sci. Lett.* **2015**, *415*, 25–37. [CrossRef]
43. Ludwig, K.R.; Cooper, J.A. Geochronology of Precambrian granites and associated U-Ti-Th mineralization, northern Olary province, South Australia. *Contrib. Mineral. Petrol.* **1984**, *86*, 298–308. [CrossRef]
44. Corfu, F.; Andrews, A.J. A U–Pb age for mineralized Nipissing diabase, Gowganda, Ontario. *Can. J. Earth Sci.* **1986**, *23*, 107–109. [CrossRef]
45. Schärer, U.; Krogh, T.E.; Gower, C.F. Age and evolution of the Grenville Province in eastern Labrador from U-Pb systematics in accessory minerals. *Contrib. Mineral. Petrol.* **1986**, *94*, 438–451. [CrossRef]
46. Mezger, K.; Hanson, G.N.; Bohlen, S.R. High-precision UPb ages of metamorphic rutile: application to the cooling history of high-grade terranes. *Earth Planet. Sci. Lett.* **1989**, *96*, 106–118. [CrossRef]
47. Corfu, F.; Muir, T.L. The Hemlo-Heron Bay greenstone belt and Hemlo Au-Mo deposit, Superior Province, Ontario, Canada 2. Timing of metamorphism, alteration and Au mineralization from titanite, rutile, and monazite U-Pb geochronology. *Chem. Geol. Isot. Geosci. Sect.* **1989**, *79*, 201–223. [CrossRef]
48. Cox, R.A.; Indares, A.; Dunning, G.R. Temperature–time paths in the high-P Manicouagan Imbricate zone, eastern Grenville Province: Evidence for two metamorphic events. *Precambrian Res.* **2002**, *117*, 225–250. [CrossRef]
49. Schmitz, M.D.; Bowring, S.A. Constraints on the thermal evolution of continental lithosphere from U-Pb accessory mineral thermochronometry of lower crustal xenoliths, southern Africa. *Contrib. Mineral. Petrol.* **2003**, *144*, 592–618. [CrossRef]
50. Rocchi, S.; Bracciali, L.; Di Vincenzo, G.; Gemelli, M.; Ghezzo, C. Arc accretion to the early Paleozoic Antarctic margin of Gondwana in Victoria Land. *Gondwana Res.* **2011**, *19*, 594–607. [CrossRef]
51. Li, Q.; Li, S.; Zheng, Y.-F.; Li, H.; Massonne, H.J.; Wang, Q. A high precision U–Pb age of metamorphic rutile in coesite-bearing eclogite from the Dabie Mountains in central China: a new constraint on the cooling history. *Chem. Geol.* **2003**, *200*, 255–265. [CrossRef]
52. Baldwin, J.A.; Bowring, S.A.; Williams, M.L.; Williams, I.S. Eclogites of the Snowbird tectonic zone: petrological and U-Pb geochronological evidence for Paleoproterozoic high-pressure metamorphism in the western Canadian Shield. *Contrib. Mineral. Petrol.* **2004**, *147*, 528–548. [CrossRef]
53. Flowers, R.M.; Bowring, S.A.; Tulloch, A.J.; Klepeis, K.A. Tempo of burial and exhumation within the deep roots of a magmatic arc, Fiordland, New Zealand. *Geology* **2005**, *33*, 17–20. [CrossRef]
54. Kylander-Clark, A.R.C.; Hacker, B.R.; Mattinson, J.M. Slow exhumation of UHP terranes: Titanite and rutile ages of the Western Gneiss Region, Norway. *Earth Planet. Sci. Lett.* **2008**, *272*, 531–540. [CrossRef]

55. Clark, D.J.; Hensen, B.J.; Kinny, P.D. Geochronological constraints for a two-stage history of the Albany–Fraser Orogen, Western Australia. *Precambrian Res.* **2000**, *102*, 155–183. [CrossRef]
56. Vry, J.K.; Baker, J.A. LA-MC-ICPMS Pb–Pb dating of rutile from slowly cooled granulites: Confirmation of the high closure temperature for Pb diffusion in rutile. *Geochim. Cosmochim. Acta* **2006**, *70*, 1807–1820. [CrossRef]
57. Storey, C.D.; Smith, M.P.; Jeffries, T.E. In situ LA-ICP-MS U–Pb dating of metavolcanics of Norrbotten, Sweden: Records of extended geological histories in complex titanite grains. *Chem. Geol.* **2007**, *240*, 163–181. [CrossRef]
58. Luvizotto, G.L.; Zack, T.; Meyer, H.P.; Ludwig, T.; Triebold, S.; Kronz, A.; Münker, C.; Stockli, D.F.; Prowatke, S.; Klemme, S.; et al. Rutile crystals as potential trace element and isotope mineral standards for microanalysis. *Chem. Geol.* **2009**, *261*, 346–369. [CrossRef]
59. Bracciali, L.; Parrish, R.R.; Horstwood, M.S.A.; Condon, D.J.; Najman, Y. U-Pb LA-(MC)-ICP-MS dating of rutile: New reference materials and applications to sedimentary provenance. *Chem. Geol.* **2013**, *347*, 82–101. [CrossRef]
60. Chew, D.M.; Petrus, J.A.; Kamber, B.S. U–Pb LA–ICPMS dating using accessory mineral standards with variable common Pb. *Chem. Geol.* **2014**, *363*, 185–199. [CrossRef]
61. Paton, C.; Hellstrom, J.; Paul, B.; Woodhead, J.; Hergt, J. Iolite: Freeware for the visualisation and processing of mass spectrometric data. *J. Anal. At. Spectrom.* **2011**, *26*, 2508–2518. [CrossRef]
62. Schmitt, A.K.; Zack, T. High-sensitivity U–Pb rutile dating by secondary ion mass spectrometry (SIMS) with an O_{2+} primary beam. *Chem. Geol.* **2012**, *332–333*, 65–73. [CrossRef]
63. Dodson, M.H. Closure temperature in cooling geochronological and petrological systems. *Contrib. Mineral. Petrol.* **1973**, *40*, 259–274. [CrossRef]
64. Dodson, M.H. Closure Profiles in Cooling Systems. *Mater. Sci. Forum* **1986**, *7*, 145–154.
65. Reiners, P.W.; Ehlers, T.A.; Zeitler, P.K. Past, Present, and Future of Thermochronology. *Rev. Mineral. Geochemistry* **2005**, *58*, 1–18. [CrossRef]
66. Heaman, L.; Parrish, R.R. U-Pb geochronology of accessory minerals. In *Applications of Radiogenic Isotope Systems to Problems in Geology, Short Course Handbook, 19*; Heaman, L., Ludden, J.N., Eds.; Mineralogical Association of Canada: Quebec City, QC, Canada, 1991; pp. 59–102.
67. Parrish, R.R. The response of mineral chronometers to metamorphism and deformation in orogenic belts. *Geol. Soc. Lond. Spec. Publ.* **2001**, *184*, 289–301. [CrossRef]
68. Hodges, K. V 3.08—Geochronology and Thermochronology in Orogenic Systems. In *Treatise on Geochemistry*; Holland, H.D., Turekian, K.K., Eds.; Pergamon: Oxford, UK, 2003; pp. 263–292. ISBN 978-0-08-043751-4.
69. Schaltegger, U.; Davies, J.H.F.L. Petrochronology of Zircon and Baddeleyite in Igneous Rocks: Reconstructing Magmatic Processes at High Temporal Resolution. *Rev. Mineral. Geochem.* **2017**, *83*, 297–328. [CrossRef]
70. Kohn, M.J.; Corrie, S.L.; Markley, C. The fall and rise of metamorphic zircon. *Am. Mineral.* **2015**, *100*, 897–908. [CrossRef]
71. Rubatto, D. Zircon: The Metamorphic Mineral. *Rev. Mineral. Geochem.* **2017**, *83*, 261–295. [CrossRef]
72. Schaltegger, U. Hydrothermal Zircon. *Elements* **2007**, *3*, 51–79. [CrossRef]
73. Cherniak, D.J.; Watson, E.B. Pb diffusion in zircon. *Chem. Geol.* **2001**, *172*, 5–24. [CrossRef]
74. Cherniak, D.J.; Watson, E.B. Diffusion in Zircon. *Rev. Mineral. Geochem.* **2003**, *53*, 113–143. [CrossRef]
75. Cherniak, D.J. Pb diffusion in rutile. *Contrib. Mineral. Petrol.* **2000**, *139*, 198–207. [CrossRef]
76. Smye, A.J.; Marsh, J.H.; Vermeesch, P.; Garber, J.M.; Stockli, D.F. Applications and limitations of U-Pb thermochronology to middle and lower crustal thermal histories. *Chem. Geol.* **2018**, *494*, 1–18. [CrossRef]
77. Kooijman, E.; Mezger, K.; Berndt, J. Constraints on the U–Pb systematics of metamorphic rutile from in situ LA-ICP-MS analysis. *Earth Planet. Sci. Lett.* **2010**, *293*, 321–330. [CrossRef]
78. Hodges, K.V.; Harries, W.E.; Bowring, S.A. 40Ar/39Ar age gradients in micas from a high-temperature-low-pressure metamorphic terrain: Evidence for very slow cooling and implications for the interpretation of age spectra. *Geology* **1994**, *22*, 55–58. [CrossRef]
79. Blackburn, T.; Bowring, S.A.; Schoene, B.; Mahan, K.; Dudas, F. U-Pb thermochronology: creating a temporal record of lithosphere thermal evolution. *Contrib. Mineral. Petrol.* **2011**, *162*, 479–500. [CrossRef]
80. Smye, A.J.; Stockli, D.F. Rutile U–Pb age depth profiling: A continuous record of lithospheric thermal evolution. *Earth Planet. Sci. Lett.* **2014**, *408*, 171–182. [CrossRef]
81. Villa, I.M. Diffusion in mineral geochronometers: Present and absent. *Chem. Geol.* **2016**, *420*, 1–10. [CrossRef]

82. Rösel, D.; Zack, T.; Boger, S.D. LA-ICP-MS U–Pb dating of detrital rutile and zircon from the Reynolds Range: A window into the Palaeoproterozoic tectonosedimentary evolution of the North Australian Craton. *Precambrian Res.* **2014**, *255*, 381–400. [CrossRef]
83. Ewing, T.A.; Rubatto, D.; Beltrando, M.; Hermann, J. Constraints on the thermal evolution of the Adriatic margin during Jurassic continental break-up: U–Pb dating of rutile from the Ivrea—Verbano Zone, Italy. *Contrib. Mineral. Petrol.* **2015**, *169*, 44. [CrossRef]
84. Bracciali, L.; Parrish, R.R.; Najman, Y.; Smye, A.; Carter, A.; Wijbrans, J.R. Plio-Pleistocene exhumation of the eastern Himalayan syntaxis and its domal 'pop-up'. *Earth-Sci. Rev.* **2016**, *160*. [CrossRef]
85. Flowers, R.M.; Mahan, K.H.; Bowring, S.A.; Williams, M.L.; Pringle, M.S.; Hodges, K. V Multistage exhumation and juxtaposition of lower continental crust in the western Canadian Shield: Linking high-resolution U-Pb and 40Ar/39Ar thermochronometry with pressure-temperature-deformation paths. *Tectonics* **2006**, *25*. [CrossRef]
86. Schoene, B.; Bowring, S.A. Determining accurate temperature–time paths from U–Pb thermochronology: An example from the Kaapvaal craton, southern Africa. *Geochim. Cosmochim. Acta* **2007**, *71*, 165–185. [CrossRef]
87. Seymour, N.M.; Stockli, D.F.; Beltrando, M.; Smye, A.J. Tracing the thermal evolution of the Corsican lower crust during Tethyan rifting. *Tectonics* **2016**, *35*, 2439–2466. [CrossRef]
88. Blackburn, T.J.; Bowring, S.A.; Perron, J.T.; Mahan, K.H.; Dudas, F.O.; Barnhart, K.R. An Exhumation History of Continents over Billion-Year Time Scales. *Science (80-.)* **2012**, *335*, 73–76. [CrossRef]
89. Smye, A.J.; Lavier, L.L.; Zack, T.; Stockli, D.F. Episodic heating of continental lower crust during extension: A thermal modeling investigation of the Ivrea-Verbano Zone. *Earth Planet. Sci. Lett.* **2019**, *521*, 158–168. [CrossRef]
90. Baldwin, J.A.; Bowring, S.A.; Williams, M.L.; Mahan, K.H. Geochronological constraints on the evolution of high-pressure felsic granulites from an integrated electron microprobe and ID-TIMS geochemical study. *Lithos* **2006**, *88*, 173–200. [CrossRef]
91. Najman, Y.; Bracciali, L.; Parrish, R.R.; Chisty, E.; Copley, A. Evolving strain partitioning in the Eastern Himalaya: The growth of the Shillong Plateau. *Earth Planet. Sci. Lett.* **2016**, *433*, 1–9. [CrossRef]
92. Mahan, K.H.; Williams, M.L.; Flowers, R.M.; Jercinovic, M.J.; Baldwin, J.A.; Bowring, S.A. Geochronological constraints on the Legs Lake shear zone with implications for regional exhumation of lower continental crust, western Churchill Province, Canadian Shield. *Contrib. Mineral. Petrol.* **2006**, *152*, 223–242. [CrossRef]
93. Martel, E.; van Breemen, O.; Berman, R.G.; Pehrsson, S. Geochronology and tectonometamorphic history of the Snowbird Lake area, Northwest Territories, Canada: New insights into the architecture and significance of the Snowbird tectonic zone. *Precambrian Res.* **2008**, *161*, 201–230. [CrossRef]
94. Dumond, G.; McLean, N.; Williams, M.L.; Jercinovic, M.J.; Bowring, S.A. High-resolution dating of granite petrogenesis and deformation in a lower crustal shear zone: Athabasca granulite terrane, western Canadian Shield. *Chem. Geol.* **2008**, *254*, 175–196. [CrossRef]
95. Flowers, R.M.; Bowring, S.A.; Mahan, K.H.; Williams, M.L.; Williams, I.S. Stabilization and reactivation of cratonic lithosphere from the lower crustal record in the western Canadian shield. *Contrib. Mineral. Petrol.* **2008**, *156*, 529. [CrossRef]
96. Hoffman, P.F. United Plates of America, The Birth of a Craton: Early Proterozoic Assembly and Growth of Laurentia. *Annu. Rev. Earth Planet. Sci.* **1988**, *16*, 543–603. [CrossRef]
97. St-Onge, M.R.; Scott, D.J.; Wodicka, N. Terrane boundaries within Trans-Hudson Orogen (Quebec–Baffin segment), Canada: changing structural and metamorphic character from foreland to hinterland. *Precambrian Res.* **2001**, *107*, 75–91. [CrossRef]
98. St-Onge, M.R.; Wodicka, N.; Lucas, S.B. Granulite and amphibolite facies metamorpism in a convergent plate margin setting: synthesis of the Quebec-Baffin segment of the Trans-Hudson Orogen. *Can. Mineral.* **2000**, *38*, 379–398. [CrossRef]
99. Parrish, R.R. U-Pb geochronology of the Cape Smith Belt and Sugluk block, northern Quebec. *Geosci. Can.* **1989**, *16*, 126–130.
100. Burg, J.-P.; Davy, P.; Nievergelt, P.; Oberli, F.; Seward, D.; Diao, Z.; Meier, M. Exhumation during crustal folding in the Namche-Barwa syntaxis. *Terra Nov.* **1997**, *9*, 53–56. [CrossRef]
101. Seward, D.; Burg, J.-P. Growth of the Namche Barwa Syntaxis and associated evolution of the Tsangpo Gorge: Constraints from structural and thermochronological data. *Tectonophysics* **2008**, *451*, 282–289. [CrossRef]

102. Finnegan, N.J.; Hallet, B.; Montgomery, D.R.; Zeitler, P.K.; Stone, J.O.; Anders, A.M.; Yuping, L. Coupling of rock uplift and river incision in the Namche Barwa–Gyala Peri massif, Tibet. *GSA Bull.* **2008**, *120*, 142–155. [CrossRef]
103. Stewart, R.J.; Hallet, B.; Zeitler, P.K.; Malloy, M.A.; Allen, C.M.; Trippett, D. Brahmaputra sediment flux dominated by highly localized rapid erosion from the easternmost Himalaya. *Geology* **2008**, *36*, 711–714. [CrossRef]
104. Booth, A.L.; Chamberlain, C.P.; Kidd, W.S.F.; Zeitler, P.K. Constraints on the metamorphic evolution of the eastern Himalayan syntaxis from geochronologic and petrologic studies of Namche BarwaConstraints on the metamorphic evolution of the eastern Himalayan syntaxis. *GSA Bull.* **2009**, *121*, 385–407. [CrossRef]
105. Enkelmann, E.; Ehlers, T.A.; Zeitler, P.K.; Hallet, B. Denudation of the Namche Barwa antiform, eastern Himalaya. *Earth Planet. Sci. Lett.* **2011**, *307*, 323–333. [CrossRef]
106. Zeitler, P.K.; Meltzer, A.S.; Brown, L.; Kidd, W.S.F.; Lim, C.; Enkelmann, E. Tectonics and topographic evolution of Namche Barwa and the easternmost Lhasa block, Tibet. In *Toward an Improved Understanding of Uplift Mechanisms and the Elevation History of the Tibetan Plateau*; Nie, J., Horton, B.K., Hoke, G.D., Eds.; Geological Society of America: Boulder, CO, USA, 2014; Volume 507, pp. 23–58. ISBN 9780813725079.
107. King, G.E.; Herman, F.; Guralnik, B. Northward migration of the eastern Himalayan syntaxis revealed by OSL thermochronometry. *Science (80-.)* **2016**, *353*, 800–804. [CrossRef]
108. Blum, M.; Rogers, K.; Gleason, J.; Najman, Y.; Cruz, J.; Fox, L. Allogenic and Autogenic Signals in the Stratigraphic Record of the Deep-Sea Bengal Fan. *Sci. Rep.* **2018**, *8*, 7973. [CrossRef]
109. Govin, G.; Najman, Y.; Copley, A.; Millar, I.; van der Beek, P.; Huyghe, P.; Grujic, D.; Davenport, J. Timing and mechanism of the rise of the Shillong Plateau in the Himalayan foreland. *Geology* **2018**, *46*, 279–282. [CrossRef]
110. Zhang, P.; Najman, Y.; Mei, L.; Millar, I.; Sobel, E.R.; Carter, A.; Barfod, D.; Dhuime, B.; Garzanti, E.; Govin, G.; et al. Palaeodrainage evolution of the large rivers of East Asia, and Himalayan-Tibet tectonics. *Earth-Sci. Rev.* **2019**, *192*, 601–630. [CrossRef]
111. Najman, Y.; Mark, C.; Barfod, D.N.; Carter, A.; Parrish, R.; Chew, D.; Gemignani, L. Spatial and temporal trends in exhumation of the Eastern Himalaya and syntaxis as determined from a multitechnique detrital thermochronological study of the Bengal Fan. *GSA Bull.* **2019**, *131*, 1607–1622. [CrossRef]
112. Warren, C.J.; Grujic, D.; Cottle, J.M.; Rogers, N.W. Constraining cooling histories: rutile and titanite chronology and diffusion modelling in NW Bhutan. *J. Metamorph. Geol.* **2012**, *30*, 113–130. [CrossRef]
113. Handy, M.R.; Franz, L.; Heller, F.; Janott, B.; Zurbriggen, R. Multistage accretion and exhumation of the continental crust (Ivrea crustal section, Italy and Switzerland). *Tectonics* **1999**, *18*, 1154–1177. [CrossRef]
114. Vavra, G.; Schmid, R.; Gebauer, D. Internal morphology, habit and U-Th-Pb microanalysis of amphibolite-to-granulite facies zircons: geochronology of the Ivrea Zone (Southern Alps). *Contrib. Mineral. Petrol.* **1999**, *134*, 380–404. [CrossRef]
115. Ewing, T.A.; Hermann, J.; Rubatto, D. The robustness of the Zr-in-rutile and Ti-in-zircon thermometers during high-temperature metamorphism (Ivrea-Verbano Zone, northern Italy). *Contrib. Mineral. Petrol.* **2013**, *165*, 757–779. [CrossRef]
116. Harrison, T.M.; Copeland, P.; Kidd, W.S.F.; Yin, A.N. Raising Tibet. *Science (80-.)* **1992**, *255*, 1663–1670. [CrossRef]
117. Reiners, P.W. Zircon (U-Th)/He Thermochronometry. *Rev. Mineral. Geochem.* **2005**, *58*, 151–179. [CrossRef]
118. Parrish, R.R.; Hodges, V. Isotopic constraints on the age and provenance of the Lesser and Greater Himalayan sequences, Nepalese Himalaya. *GSA Bull.* **1996**, *108*, 904–911. [CrossRef]
119. DeCelles, P.G.; Gehrels, G.E.; Quade, J.; LaReau, B.; Spurlin, M. Tectonic Implications of U-Pb Zircon Ages of the Himalayan Orogenic Belt in Nepal. *Science (80-.)* **2000**, *288*, 497–499. [CrossRef]
120. Najman, Y. The detrital record of orogenesis: A review of approaches and techniques used in the Himalayan sedimentary basins. *Earth-Sci. Rev.* **2006**, *74*, 1–72. [CrossRef]
121. Grujic, D.; Coutand, I.; Bookhagen, B.; Bonnet, S.; Blythe, A.; Duncan, C. Climatic forcing of erosion, landscape, and tectonics in the Bhutan Himalayas. *Geology* **2006**, *34*, 801–804. [CrossRef]
122. Zeitler, P.K.; Koons, P.O.; Bishop, M.P.; Chamberlain, C.P.; Craw, D.; Edwards, M.A.; Hamidullah, S.; Jan, M.Q.; Khan, M.A.; Khattak, M.U.K.; et al. Crustal reworking at Nanga Parbat, Pakistan: Metamorphic consequences of thermal-mechanical coupling facilitated by erosion. *Tectonics* **2001**, *20*, 712–728. [CrossRef]

123. Gehrels, G.; Kapp, P.; DeCelles, P.; Pullen, A.; Blakey, R.; Weislogel, A.; Ding, L.; Guynn, J.; Martin, A.; McQuarrie, N.; et al. Detrital zircon geochronology of pre-Tertiary strata in the Tibetan-Himalayan orogen. *Tectonics* **2011**, *30*. [CrossRef]
124. Hodges, K. V Tectonics of the Himalaya and southern Tibet from two perspectives. *GSA Bull.* **2000**, *112*, 324–350. [CrossRef]
125. Hu, X.; Garzanti, E.; Wang, J.; Huang, W.; An, W.; Webb, A. The timing of India-Asia collision onset – Facts, theories, controversies. *Earth-Sci. Rev.* **2016**, *160*, 264–299. [CrossRef]
126. Najman, Y.; Jenks, D.; Godin, L.; Boudagher-Fadel, M.; Millar, I.; Garzanti, E.; Horstwood, M.; Bracciali, L. The Tethyan Himalayan detrital record shows that India–Asia terminal collision occurred by 54 Ma in the Western Himalaya. *Earth Planet. Sci. Lett.* **2017**, *459*. [CrossRef]
127. Allen, R.; Najman, Y.; Carter, A.; Barfod, D.; Bickle, M.J.; Chapman, H.J.; Garzanti, E.; Vezzoli, G.; Ando, S.; Parrish, R.R. Provenance of the Tertiary sedimentary rocks of the Indo-Burman Ranges, Burma (Myanmar): Burman arc or Himalayan-derived? *J. Geol. Soc. Lond.* **2008**, *165*, 1045–1057. [CrossRef]
128. Maurin, T.; Rangin, C. Structure and kinematics of the Indo-Burmese Wedge: Recent and fast growth of the outer wedge. *Tectonics* **2009**, *28*. [CrossRef]
129. Licht, A.; Dupont-Nivet, G.; Win, Z.; Swe, H.H.; Kaythi, M.; Roperch, P.; Ugrai, T.; Littell, V.; Park, D.; Westerweel, J.; et al. Paleogene evolution of the Burmese forearc basin and implications for the history of India-Asia convergence. *GSA Bull.* **2018**, *131*, 730–748. [CrossRef]
130. Galy, A.; France-Lanord, C. Higher erosion rates in the Himalaya: Geochemical constraints on riverine fluxes. *Geology* **2001**, *29*, 23–26. [CrossRef]
131. Vermeesch, P. Quantitative geomorphology of the White Mountains (California) using detrital apatite fission track thermochronology. *J. Geophys. Res. Earth Surf.* **2007**, *112*. [CrossRef]
132. Cawood, P.A.; Johnson, M.R.W.; Nemchin, A.A. Early Palaeozoic orogenesis along the Indian margin of Gondwana: Tectonic response to Gondwana assembly. *Earth Planet. Sci. Lett.* **2007**, *255*, 70–84. [CrossRef]
133. Harrison, T.M.; Zeitler, P.K. Fundamentals of Noble Gas Thermochronometry. *Rev. Mineral. Geochemistry* **2005**, *58*, 123–149. [CrossRef]
134. Carrapa, B. Resolving tectonic problems by dating detrital minerals. *Geology* **2010**, *38*, 191–192. [CrossRef]
135. Henderson, A.L.; Najman, Y.; Parrish, R.; Mark, D.F.; Foster, G.L. Constraints to the timing of India–Eurasia collision; a re-evaluation of evidence from the Indus Basin sedimentary rocks of the Indus–Tsangpo Suture Zone, Ladakh, India. *Earth-Sci. Rev.* **2011**, *106*, 265–292. [CrossRef]
136. Lang, K.A.; Huntington, K.W.; Burmester, R.; Housen, B. Rapid exhumation of the eastern Himalayan syntaxis since the late Miocene. *GSA Bull.* **2016**, *128*, 1403–1422. [CrossRef]
137. Gemignani, L.; van der Beek, P.A.; Braun, J.; Najman, Y.; Bernet, M.; Garzanti, E.; Wijbrans, J.R. Downstream evolution of the thermochronologic age signal in the Brahmaputra catchment (eastern Himalaya): Implications for the detrital record of erosion. *Earth Planet. Sci. Lett.* **2018**, *499*, 48–61. [CrossRef]
138. Kohn, M.J. Himalayan Metamorphism and Its Tectonic Implications. *Annu. Rev. Earth Planet. Sci.* **2014**, *42*, 381–419. [CrossRef]
139. Guo, Z.; Wilson, M. The Himalayan leucogranites: Constraints on the nature of their crustal source region and geodynamic setting. *Gondwana Res.* **2012**, *22*, 360–376. [CrossRef]
140. Guo, Z.; Wilson, M. Late Oligocene–early Miocene transformation of postcollisional magmatism in Tibet. *Geology* **2019**, *47*, 776–780. [CrossRef]
141. Mitchell, A.; Chung, S.-L.; Oo, T.; Lin, T.-H.; Hung, C.-H. Zircon U–Pb ages in Myanmar: Magmatic–metamorphic events and the closure of a neo-Tethys ocean? *J. Asian Earth Sci.* **2012**, *56*, 1–23. [CrossRef]
142. Gardiner, N.J.; Searle, M.P.; Morley, C.K.; Robb, L.J.; Whitehouse, M.J.; Roberts, N.M.W.; Kirkland, C.L.; Spencer, C.J. The crustal architecture of Myanmar imaged through zircon U-Pb, Lu-Hf and O isotopes: Tectonic and metallogenic implications. *Gondwana Res.* **2018**, *62*, 27–60. [CrossRef]
143. Ji, W.-Q.; Wu, F.-Y.; Chung, S.-L.; Li, J.-X.; Liu, C.-Z. Zircon U–Pb geochronology and Hf isotopic constraints on petrogenesis of the Gangdese batholith, southern Tibet. *Chem. Geol.* **2009**, *262*, 229–245. [CrossRef]
144. Ji, W.-Q.; Wu, F.-Y.; Liu, X.-C.; Liu, Z.-C.; Zhang, C.; Liu, T.; Wang, J.-G.; Paterson, S.R. Pervasive Miocene melting of thickened crust from the Lhasa terrane to Himalaya, southern Tibet and its constraint on generation of Himalayan leucogranite. *Geochim. Cosmochim. Acta* **2019**. [CrossRef]

145. Yang, L.; Liu, X.-C.; Wang, J.-M.; Wu, F.-Y. Is Himalayan leucogranite a product by in situ partial melting of the Greater Himalayan Crystalline? A comparative study of leucosome and leucogranite from Nyalam, southern Tibet. *Lithos* **2019**, *342–343*, 542–556. [CrossRef]
146. France-Lanord, C.; Spiess, V.; Klaus, A.; Schwenk, T.; Schwenk, T.; The Expedition 354 Scientists. Expedition 354 summary. *Proc. Int. Ocean Discov. Progr.* **2016**, *354*, 1–35.
147. Cochrane, R.; Spikings, R.A.; Chew, D.; Wotzlaw, J.-F.; Chiaradia, M.; Tyrrell, S.; Schaltegger, U.; Van der Lelij, R. High temperature (>350 °C) thermochronology and mechanisms of Pb loss in apatite. *Geochim. Cosmochim. Acta* **2014**, *127*, 39–56. [CrossRef]
148. Frei, R.; Villa, I.M.; Nägler, T.F.; Kramers, J.D.; Przybylowicz, W.J.; Prozesky, V.M.; Hofmann, B.A.; Kamber, B.S. Single mineral dating by the PbPb step-leaching method: Assessing the mechanisms. *Geochim. Cosmochim. Acta* **1997**, *61*, 393–414. [CrossRef]
149. Kramers, J.; Frei, R.; Newville, M.; Kober, B.; Villa, I. On the valency state of radiogenic lead in zircon and its consequences. *Chem. Geol.* **2009**, *261*, 4–11. [CrossRef]